Characterization of a 3D Printed Pumped Counterflow Virtual Impactor and an Aerodynamic Lens Concentrator

by

Libby Koolik

Submitted to the
Department of Earth, Atmospheric, and Planetary Sciences
in Partial Fulfillment of the Requirements for the Degree of

Bachelor of Science

at the

Massachusetts Institute of Technology

February 2017

Signature of Author Signature redacted
Department of Earth, Atmospheric, and Planetary Science
December 19, 2016

Certified by Signature redacted
Daniel Cziczo
Associate Professor of Atmospheric Chemistry
Thesis Supervisor

Accepted by Signature redacted
Richard P. Binzel
Professor of Planetary Sciences and Margaret MacVicar Faculty Fellow
Undergraduate Officer

Characterization of a 3D Printed Pumped Counterflow Virtual Impactor and an Aerodynamic Lens Concentrator

By Libby P. Koolik

Candidate for a Bachelor's of Science Degree in
Earth, Atmospheric, and Planetary Science
December 2016

Abstract

Atmospheric aerosols have an important role in cloud formation and, by extension, in the overall climate system. Field studies are required to refine the uncertainty associated with the net radiative effect of atmospheric aerosols. Two pre-existing cloud sampling devices, the pumped counterflow virtual impactor (PCVI) and aerodynamic lens concentrator (ADL), were modelled using computer aided design software and printed using stereolithography printing. These devices were compared against their industrial counterparts. The printed PCVI was proven to be as effective as the industrial PCVI in a smaller working range. The printed concentrator effectively concentrated particles, but at a lower concentration factor than the industrial concentrator. This study revealed potential for further refinement in design features for both devices and it served as an essential pre-study for future field campaigns that will use these 3D printed devices.

Introduction

The stalemate in political action combating climate change is often attributed to the scientific uncertainty in the climate system (Boucher et al., 2013; Kupiszewski et al., 2015). While there is almost unanimous scientific agreement that the Earth's climate is changing, the largest portion of this uncertainty is due to the effects of aerosols on clouds (Boucher et al., 2013).

Clouds interact with the climate system via a complicated and paradoxical process, making it hard to characterize their net effect; while they are high albedo surfaces that reflect light and cool the planet, they are often made of water vapor, a greenhouse gas warming agent (Boucher et al., 2013; Lohmann, Lüönd, & Mahrt, 2016). There is a large push in the scientific community to better understand the role of cloud formation on the global climate system and to characterize the way that clouds are changing and will be changing as humans continue to have a profound effect on the environment (Boucher et al., 2013).

Clouds are the result of phase transitions from gaseous water vapor to liquid water droplets or solid ice crystals (Lohmann et al., 2016). The formation of droplets from the vapor phase is often achieved through aerosol nucleation, which occurs when the gaseous water vapor is in a metastable state and overcomes the energy barrier required for phase shifting by forming clusters of droplets around an aerosol (Lohmann et al., 2016). These aerosols are referred to as cloud condensation nuclei (CCN). At temperatures below the freezing point of water, aerosols can also act as ice nucleating particles (INP). As humans continue to influence the environment through pollution, they are affecting the assortment of atmospheric aerosols, CCNs, and INPs; this impacts the cloud cover and therefore also the climate (DeMott et al., 2010; Fuzzi et al., 2015). To best understand the role of clouds in the climate system, the scientific community must also understand the evolving physical and chemical properties of these clouds.

To achieve this, we need to develop the necessary tools to study these CCNs and INPs one particle at a time. Only by sampling a cloud and analyzing the specific particles that formed it, can we truly begin to understand its chemical and microphysical properties. In the process, we need to be able to sample particles at high concentrations and separate the interstitial particles from the ones which acted as CCN or INP. Additionally, these particles exist in the atmosphere at very low concentrations, so concentration enhancement is required for more effective sampling. A concentrator (ADL, Enertechnix) can be used to increase the number concentration of sample particles while the separation can be achieved by using a Pumped Counterflow Virtual Impactor (PCVI).

Amplification of particle count can be done by using a concentrator consisting of a series of sharp-edge size-decreasing contractions. The particle-laden flow is concentrated in central streamlines, while the bulk flow of particle-free gas is pumped away on the outer ring of the concentrator. As a result, the sample flow out of the concentrator is a small fraction of the original gas that contained particles. Concentration ratios as high as 50:1 can be achieved (Enertechnix Manual of Operation, 2010).

Once the particle count is amplified for a larger sample of particles per volume, it is important that the particles be separated based on size so that only the particles that nucleated clouds will be analyzed (Slowik, Cziczo, & Abbatt, 2011). This technique has been used in a large number of studies since the mid-1980s when Ogren et al. (1985) first described a technique of using aerodynamic properties to separate atmospheric trace gases from cloud droplets.

In its original stage of development, this technology was mostly used on airplanes to take in-situ measurements of clouds. The Counterflow Virtual Impactor (CVI) is a device that harnesses the airflow created by aircraft movement to sample and size-select particles (Lin & Heintzenberg, 1995; Ogren et al., 1985). The key is the creation of a stagnation plane, a line in space where airflow streamline velocity is zero (Lin & Heintzenberg, 1995). The stagnation plane makes it such that only particles with sufficient inertia – those that are large enough – can propel themselves past this area of no velocity.

In 2006, this technique was expanded to a ground-based sampling method using vacuum-pumped air to generate the flow required to create a stagnation plane instead of an aircraft (Boulter et al., 2006; Hiranuma et al., 2016). Boulter et al. (2006) designed the PCVI apparatus to perform the same measurements without an airplane or wind tunnel. The uses a vacuum pump to provide a "pump flow," an air pump to introduce an "add flow," and at each end there is an "input flow" and "output flow" or "sample flow" (Boulter et al., 2006). Together, the add flow and pump flow create an "effective counterflow" which counteracts the input flow. A schematic adapted from Boulter et al. (2006) is included in Figure 1 for reference.

The add flow and pump flow values regulate the cutoff size of aerosols that can pass through the PCVI. The 50% cut size or "D50" describes the lower bound of particle size that is transmitted through the PCVI at a 50% transmission efficiency. For the PCVI to work, the add flow must be larger than the output flow (Boulter et al., 2006; Kulkarni et al., 2011). This is necessary to create the effective counterflow, which creates the stagnation plane. The effective counterflow is defined as the add flow minus the output flow (Kulkarni et al., 2011). The other critical flow value that can be adjusted to change the particle cut size is the input flow into the PCVI, which can be adjusted by changing the pump flow. In many cases, this input flow is dependent on the other flows when doing sampling (Kulkarni et al., 2011; Slowik et al., 2011)

The PCVI can also act as a size-separating concentrator in a similar manner as the concentrator. The PCVI removes the input gas and all particles smaller than the D50. Particles

larger than the D50 will be entrained into the sample flow where the carrier gas is only made of the add flow. The enhancement should be roughly equal to the ratio of input to output flows (Slowik et al., 2011), though it is possible that it could exceed this theoretical enhancement factor. Performance studies and numerical model analyses were performed on both the CVI and PCVI. With both devices, the numerical models showed that the theoretical streamlines and performance aligned very well with the experimental results (Kulkarni et al., 2011; Lin & Heintzenberg, 1995).

Since the original characterizations by Boulter et al. (2006) and Kulkarni et al. (2011), the PCVI has been used in many studies. One example was Slowik et al. (2011). In this study, Slowik et al. (2011) described a system for characterizing CCN using a PCVI. It is cited that it would not be possible to do this type of measurement without a PCVI (Slowik et al., 2011). The PCVI was also cited to be useful in other recent studies (examples: Baustian et al., 2012; Friedman et al., 2013).

Based on computational fluid dynamic ("CFD") modelling, Kulkarni et al. (2011) suggested potential improvements on the PCVI. By harnessing the power of 3D modelling and printing, there is great potential for future advances. The suggested five aspects of improvement: redesign of nozzle free jet surface to minimize loss due to turbulence; redesign of nozzle geometry to reduce non-uniform counterflow velocity; adjustment of nozzle length and angle to maximize transmission efficiency; usage of a mixing volume to make output more homogeneous; and improved understanding of effects on complex, non-spherical shaped particles. The 3D modelling software and ease-of-printing should allow these improvements and others to be carried out.

Future projects for the PCVI and CVI systems are aimed towards solving the challenge behind understanding mixed-phase cloud formation. Mixed-phase clouds are found between 0 to -38°C and cannot be rigorously studied with a single CVI or PCVI (Lohmann et al., 2016; Mertes et al., 2007). This occurs because these clouds have both ice crystals and water droplets and thus a diverse set of CCN. Additionally, ice crystals affect both the lifetime and albedo of a cloud, so they have a distinct role in the overall climate system than purely droplet-based clouds (Mertes et al., 2007). It is also proposed that the properties of ice nucleating particles (INP) for mixed phase clouds are distinct from upper tropospheric INP (Mertes et al., 2007). Another reason that these clouds are particularly important is their atmospheric prevalence; an 11-year study from Germany showed that mixed-phase clouds make up roughly 12% of clouds (Seifert et al., 2010). It is thus important that we understand the mechanism by which they form in order to better understand the evolving atmospheric cloudscape.

The Ice-CVI is a ground-based, vertically-aligned system that uses a series of virtual impactors to segregate particles based on size and water phase (Mertes et al., 2007). The Ice-CVI system is an attempt to separate ice crystal-forming from cloud droplet-condensing from interstitial aerosols based solely on size (Mertes et al., 2007). The basic design incorporates four stacked components to parse through air with ice crystals, super cooled droplets, and interstitial aerosols to leave only small ice particles: the omni-directional inlet and virtual impactor remove precipitation and particles larger than 20 μm, the pre-impactor uses impact freezing to remove super cooled droplets, and the CVI at the base removes all small interstitial particles as was installed at the Jungfraujoch research station (Mertes et al., 2007).

Another system that incorporates PCVI/CVI technology is the Ice Selecting PCVI or "IS-PCVI" as described by Hiranuma et al. (2016). The PCVI in the IS-PCVI setup works like the PCVI described in Kulkarni et al. (2011) but at a larger scale (Hiranuma et al., 2016). Due to its

larger size, the IS-PCVI can achieve cut sizes as high as 30 μm, as opposed to the traditional PCVI which has an upper bound around 5 μm (Hiranuma et al., 2016).

The potential applications for this technology are vast, but the cost is a barrier to entry for many groups who may want to use these instruments. The commercially available version of the PCVI has a few issues aside from cost. The PCVI, for example, has a very delicate inlet nozzle causing particle losses and a reduction in transmitted particles if misaligned. There are also limitations on classical machining when building a complex instrument like a PCVI or a concentrator. The usage of a 3D stereolithography (SLA) printer can solve some of these problems: the photopolymer resin required for each part is less expensive than the cost of a machined part, the inlet nozzle can be printed with a thicker outer diameter to increase stability, and most importantly the entire part can be printed in a single piece which reduces misalignment as opposed to the three-piece industrial counterpart. For those reasons, a 3D SLA printer can increase both access and ability of these instruments for many research groups.

In this study, a concentrator and a PCVI were designed, 3D printed, and compared to their commercial counterparts. This is an essential pre-study for an upcoming project in which a phase separation inlet system including a concentrator and a PCVI for sampling mixed-phase clouds will be built. Findings from these future measurements will hopefully improve our understanding of particles acting as CCN and/or INP in the atmosphere and eventually our understanding of the role of aerosols on clouds and on the overall climate system.

Design Methods

The ADL Concentrator (Enertechnix) and PCVI (Model 8100, BMI, Inc.) specifications were referenced to create similar models in Solidworks. Drawings used to print the 3D models are included for reference in the appendix. The drawings were exported from Solidworks to Preform, a software created by Formlabs to communicate with their printers. The created models were printed using a 3D SLA printer (Form2, Formlabs Inc.). It uses a 405 nm UV laser beam to selectively cure specific locations in the resin bath on each layer (Formlabs, 2015). For each vertical layer of the drawing, the laser beam cures a cross section of the design from liquid to solid. The Form2 can print at 25, 50, and 100-micron layer thickness resolution (Formlabs, 2015); for these experiments, the concentrator and PCVI were printed at a 100-micron resolution using clear resin. The resin used has a tensile strength of 65 MPa (Formlabs, 2014). After printing was completed, the pieces were completed by removing the structural support and rinsing the pieces in isopropyl alcohol for twenty minutes before placing it in an UV-Box containing LED lights at the same wavelength as the printer's laser to post-cure the printed parts (Roesch et al., 2016, submitted to AMT).

Experimental Setup

The data on particle size and number concentration were collected using the Optical Particle Sizer (OPS, Model 3330, TSI). The OPS uses single particle optical scattering to measure the size of and count particles as they flow through the system at a regulated constant flow rate of 1.0 LPM (TSI, 2011, pp. 1–3). An internal laser beam is used to illuminate the particles for light scattering. After scattering, the OPS classifies particles into sixteen distinct bins based on particle diameter. These bins range from 0.3 to 10 μm. The results are then communicated through the Aerosol Instrument Manager software designed by TSI and analyzed using Microsoft Excel, MATLAB, and Origin.

Flows were controlled by mass flow controllers (MFC, MCS Series, Alicat) and verified by a gas flow calibrator (Bios, DryCal Definer 220, Mesa Laboratories). The MFC are accurate within +/-0.8% of their reported flow rates (Alicat Scientific, 2016). The Bios reports standard flow rates within +/-1% accuracy and volumetric flow rates within +/- 0.75% accuracy (Mesa Laboratories, 2015). For both experiments, filtered compressed air was used to generate particles, the OPS flow, and supply the add flow for the PCVI.

Particles for both experiments were generated using a bubble burst generator ("bubbler"), a flask with a porous frit. This system works by mimicking the bubble burst process by which sea salt becomes aerosolized. Pressurized air at a constant and controlled flow rate is pushed through the porous frit into the ammonium sulfate solution, which causes the solution to bubble. When the bubbles burst, the aerosol is released into the air flow that enters the experimental system. In both experiments, the particle-laden flow was passed through a silica gel diffusion drier to remove any condensed water that would skew the size selection of particles by artificially increasing the size.

The experimental setups used to characterize the concentrators are shown in Figure 2. For this study, a concentration of 0.1 g/L ammonium sulfate was used. The bubbler was characterized to show constant output after a warm-up period of 30 minutes. The results of this characterization are summarized in Figure 3. Before any experiments, the bubbler warmed up for 30 minutes.

A series of twelve five-minute experiments were performed on each concentrator. Each concentrator was run for five minutes in the reference setup (Figure 2A) with the pump flow outlet plugged and a constant excess flow controlled by a MFC. The excess flow rate in the reference test corresponded to the Pump flow for the sample run. Samples were collected at a 1-second resolution over the 16 size bins in the OPS. After the five-minute period ended, the apparatus was changed to the sample setup by removing the flow splitter and connecting the Pump flow to the concentrator. The sample run would similarly collect samples at a 1-second resolution over the 16 size bins. Before both the reference and sample tests, the flow into the concentrator was measured by the Bios DryCal Definer and recorded for consistency.

The PCVI tests were performed using the measurement setups shown in Figure 4. A concentration of 0.1 g/L ammonium sulfate was used and aerosols were generated using the same bubbler system. A series of sixteen measurements were performed on each PCVI. Six measurements used three volumetric input flow values cited by Kulkarni 2011. The results of these tests were then compared to those referenced in the literature. The remaining ten measurements were performed using five standard pump flow rates in order to provide a proper characterization of cut sizes over a scale of different input flows. For these measurements, the sample flow and add flow were kept constant.

Investigating the input flow rate from the sample run provided the required input flow for the reference run. Before the sample test, the Bios was used to measure the input flow into the PCVI. The excess flow in the reference test was adjusted such that the input flow into the PCVI matched that of the sample test. The transmission efficiencies were later adjusted by this input flow to output flow ratio.

Once the results were collected, the transmission efficiency was calculated for each PCVI at each flow rate by dividing the average sample results by the average reference results for each bin size over the five-minute sampling period.

$$(1)\ Transmission\ Efficiency = \frac{Average\ Sample\ Concentration}{Average\ Reference\ Concentration}$$

Afterward, the transmission efficiency was corrected for the input flow to output flow ratio to prevent false concentration enhancement.

$$(2)\ Corrected\ Transmission\ Efficiency = \frac{Transmission\ Efficiency}{Input\ Flow/Output\ Flow}$$

Finally, the corrected transmission efficiencies were plotted against median particle diameter, and a sigmoidal curve was fitted to the data to find the 50% transmission efficiency diameter. This analysis was performed in Origin.

Results

CONCENTRATOR

The results of one of the experiments on the industrial concentrator is shown in Figure 5. The plot shown is the result of the 4 SLPM pump flow scenario. The data shown are the result of the sample run divided by the reference run, referred to as the concentration factor, over the size range from 0-2 μm. The dashed red curve is a sigmoidal fit of the data in this range and the height at which it levels off is marked with a solid blue line. The height of the blue line is the concentration enhancement factor for the specific flow regime. (The error was calculated as standard deviation, adjusted using the division of standard deviations formula, but it was left off of these curves in order to cleanly present the data. It is available upon request.) The curves for the other flow scenarios are included in the appendix.

A similar plot is shown in Figure 6 where the same experiment was performed on the printed concentrator using the same flow scenario. Note that there is a difference in scale between the two plots. The crucial aspect of the plot is the shape, not the height, so the difference in scaling is merely to best display the shape of the data.

Figure 7 displays the concentration enhancement factor in the 1-2 μm diameter range for different pump flow values for the industrial concentrator and for the printed concentrator over the 5-minute experiments. These results are also summarized in Table 1. The individual concentration factor curves for each pump flow can be found in the appendix. In trials where there was no asymptotic behavior in this size range, an approximate value was calculated by taking the average of the concentration factors in the 1-2 μm range. These results are plotted without the red sigmoidal curve in the appendix. Note that the concentration factors are being plotted on different y-axes due to the difference in scale between the two results. The results have nevertheless been plotted together to draw comparisons in overall trend.

PCVI

Figure 8A shows the results of the corrected transmission efficiency for an input flow of 11.97 LPM in the industrial PCVI. (Again, error bars have been removed to best highlight the shape of the curve. Standard deviations adjusted for the calculations can be accessed upon specific request.) The dashed red curve is a sigmoidal fit to the data, neglecting outliers in the larger size bins. These data points will be neglected because the calculated transmission efficiency is artificially high due to low concentration at larger particle sizes. The D50 is shown in the inset plot in Figure 8B. The thin gray line indicates the 50% transmission point efficiency. The thick blue line shows the D50, which is the intersection between the red dashed line and the thin gray line.

This analysis was performed for each of the experiments with the industrial concentrator and the resulting D50 values are summarized in Table 2. Figure 9 shows the results of the input flow versus D50 for the industrial PCVI. The individual transmission curves for the other flow values are included in the appendix.

A similar curve for an input flow of 11.97 LPM for the printed PCVI is shown in Figure 10. Note that there is a difference in scale for the large plot than is shown for the industrial PCVI. The printed PCVI was found to be very effective at size-separating particles within a specific range of pump flows. With a constant add flow of 2.0 SLPM and a constant sample flow of 0.87 SLPM, the PCVI had a working range between pump flows of 5 and 7.5 SLPM.

A comparison of the industrial and printed PCVI D50 versus input flow is shown in Figure 11. Only three of the flow scenarios performed in standard liters per minute (SLPM) were compared from the industrial PCVI tests to the printed PCVI tests due to the working range of functioning the printed PCVI. These results were obtained and analyzed using the same apparatus and process. The results were very similar between the two PCVI devices, showing that the printed PCVI functions very similarly to the industrial one.

The results of the measurements performed on the printed PCVI using flow rates from Kulkarni et al. (2011) are shown in Table 3 and compared with the results reported in the literature.

Discussion

CONCENTRATOR

The analysis was performed with the 1-2 μm diameter range in order to consistently capture the concentration enhancement jump that occurs around 1 μm diameter. This limitation can be justified in two ways. First, this is an important size range of atmospheric particles and consequently relevant for concentrating. Second, the concentration factors for particles larger than 2 μm are noisy due to low particle counts in these larger bins during the reference tests.

The printed concentrator did not have a good sigmoidal shape in the 0-2 μm range for any of the flow scenarios, so the average concentration factor from 1-2 μm was calculated for each flow scenario. This is a fair and moderately conservative approximation of the standard concentration enhancement factor because this region captures the range in which the concentrator changes from not concentrating to concentrating, usually with a steep increase. Additionally, this region has consistent and high particle counts for the reference run, so it is not at risk of artificial enhancement due to low particle count. In many cases, the concentrator reached higher concentration at larger particle sizes, but this could be due to lower particle count and noise. If the plots were zoomed out to include particles of all size bins, the printed concentrator also exhibited sigmoidal behavior as it approached the 5 μm particles. In this sense, both concentrators performed as theorized.

The industrial concentrator performed approximately to the concentration factor reported by Enertechnix, and the printed concentrator worked but at a lower concentration factor. At the highest pump flow, the industrial concentrator reached an approximate concentration factor of 40, which is close to the reported 50:1 ratio. At the highest pump flow, the printed concentrator reached an approximate concentration factor of 3. Both of these values refer only to the

concentration factor achieved in the 0-2 μm range; at higher particle diameters, higher concentration factors were reached with both.

The trend for both the industrial and printed concentrator was similar and showed an increase in concentration factor with increased flow rate. While the industrial concentrator had a steeper increase and higher concentration factors overall, the printed concentrator followed the same general trend.

PCVI

The individual transmission efficiency curves for both the industrial and the printed PCVI demonstrated the idealized behavior as described in Boulter et al. (2006) and Kulkarni et al. (2011). Sigmoidal curves fit the data with R^2 values that approached roughly 1 for all pump flows. In many cases, the last few size bins were neglected due to the assumption that particles in size bins larger than the D50 were collected with a 100% transmission efficiency.

There was a large amount of uncertainty in small particle diameter size bins. This can be attributed to inadvertent transmission of small particles in the wake of larger ones. For this reason, there is not as high of an error in the sizes larger than the D50, where the particle count is much more consistent.

It is important to note that the corrected transmission efficiency exceeds 1.0 in many of the individual curves. This is due to the ability of the PCVI to act as a concentrator. In the same way that the concentrator enhances particle concentration by pumping away major flows that are particle-free, the PCVI also amplifies the concentration of particles.

For the three flow scenarios shown in Figure 11 in which the industrial and printed PCVIs functioned properly, the D50 values were in the same range. At the core of the printed PCVI's working range (input flow of roughly 4.5 SLPM), the printed and industrial PCVI had almost the exact same D50 values.

Additionally, the tests performed with constant add flow in Figure 11 demonstrated the idealized relationship by which cut size increases with decreasing input flow. This is shown in the industrial PCVI characterization plot (Figure 9).

The comparison in Table 3 of the printed PCVI D50 values for the Kulkarni et al. (2011) flow rates is noteworthy. In almost all cases, the printed PCVI cut at a smaller size than the Kulkarni PCVI. In the only two flow scenarios where the D50 was larger, the printed PCVI D50 was within 5% difference of the literature value. The trend between data points is consistent as well.

The lower cut sizes in the printed PCVI can be attributed to a few design modifications as demonstrated in the cross sections in the Appendix. First, the input nozzle of the PCVI was smoothened to allow a more gradual entrance into the PCVI. The length of the nozzle remained consistent with the specifications discussed in Kulkarni et al. (2011). Another similar modification was made to the add flow region. To avoid blockage of the add flow pathway due to resin residue, the add flow inlet was thickened at the base and smoothened around the side of the PCVI center. The diameter of the entrance to the main body of the PCVI was kept constant to ensure that the add flow would enter with the proper velocity. The last modification made was a change in the converging angle of the input nozzle. Kulkarni et al. (2011) uses a converging

angle (θ) of 45°. As proposed in the literature, the printed PCVI had a smoothed inlet nozzle that had a slow convergence from the initial diameter to the inner diameter.

Conclusion

Both the industrial and printed versions of the concentrator and the PCVI were evaluated. Each of the four devices was characterized over a range of flow scenarios. The industrial and printed concentrators were tested using the exact same flow scenarios in the same experimental setup. While the results did not match exactly, the overall trend for both devices matched; with higher pump flow, the concentration factor increased.

For the PCVI tests, there are a few important summaries. First, both the industrial PCVI and printed PCVI displayed the theoretical behavior and demonstrated increasing cut size with decreasing input flow for the experiments where add flow was held constant. Additionally, both PCVIs showed (either in the 0-2 μm range or over the full range) the theoretical sigmoidal shape. Next, the comparison of the printed PCVI with the Kulkarni et al. (2011) results showed that the printed PCVI is either on par with or cutting particle sizes smaller than the literature values. All of these prove that the printed PCVI functions as it was designed.

There are modifications that could still be made to both printed devices. Kulkarni et al. (2011) proposes lengthening the input nozzle. According to computational fluid dynamics (CFD) model experiments performed by Kulkarni et al. (2011), an increase in nozzle length by a factor of 2.5 can lower the 50% transmission efficiency particle diameter. The use of SLA printing coupled with CFD modelling can help determine the ideal input nozzle and angle for achieving superior transmission efficiencies.

While there are no proposed modifications to the physical design of the concentrator, the best improvement for the concentrator is wider access. In current research, there is often a need to amplify the concentration of particles since ambient aerosol concentrations are very low. Many studies would benefit from having an ADL concentrator, which would help collect a higher concentration of particles for analysis.

The next phase for the 3D-printed concentrator and PCVI is to create a system that will simultaneously sample CCN, INP, and interstitial aerosols. By using SLA printing, PCVIs can be printed in various sizes to achieve the ideal cut sizes needed for this system. The system will operate by using two distinct PCVIs of different sizes. The ability to print PCVIs allows this to be done in a relatively inexpensive and timely manner, and it allows the researchers to engineer the PCVIs to select for the desired D50s. Additionally, a concentrator can be placed at the inlet of the system to amplify the concentration of particles that enter. By harnessing the concentrator in line with two PCVIs and a thermodynamic freezing chamber, comprehensive studies on atmospheric aerosols can be conducted.

Once this system is proven to function efficiently, this technology can be used to perform studies in many parts of the world under different types of cloud cover. With sufficient data, the results can be integrated into global climate models and used to understand the changing climate.

There is great potential for using SLA printing technology in atmospheric sampling devices. The results summarized above are just a first step in making atmospheric research easier, less expensive, and more efficient.

Acknowledgements

I would like to thank my advisor Dr. Dan Cziczo for his help in preparing this project and for his support as a research supervisor. I would also like to thank Dr. Michael Roesch for his direct supervision and help throughout the project. For her writing and presentation assistance, I would like to thank Jane Connor. Finally, I would like to thank all members of the Cziczo Group and Department of Earth, Atmospheric, and Planetary Sciences for their support through my MIT career.

References

Alicat Scientific. (2016). Technical Data for Alicat MC and MCR Mass Flow Controllers, *30*, 1–5.

Baustian, K. J., Cziczo, D. J., Wise, M. E., Pratt, K. A., Kulkarni, G., Hallar, A. G., & Tolbert, M. A. (2012). Importance of aerosol composition, mixing state, and morphology for heterogeneous ice nucleation: A combined field and laboratory approach. *Journal of Geophysical Research Atmospheres*, *117*(6), 1–13. https://doi.org/10.1029/2011JD016784

Boucher, O., Randall, D., Artaxo, P., Bretherton, C., Feingold, G., Forster, P., … Zhang, X.-Y. (2013). Clouds and Aerosols. In *Climate Change 2013: The Physical Science Basis. Contribution of Working Group I to the Fifth Assessment Report of the Intergovernmental Panel on Climate Change* (pp. 571–657). Cambridge.

Boulter, J. E., Cziczo, D. J., Middlebrook, A. M., Thomson, D. S., & Murphy, D. M. (2006). Design and Performance of a Pumped Counterflow Virtual Impactor. *Aerosol Science and Technology*, *40*(11), 969–976. https://doi.org/10.1080/02786820600840984

DeMott, P. J., Prenni, A. J., Liu, X., Kreidenweis, S. M., Petters, M. D., Twohy, C. H., … Rogers, D. C. (2010). Predicting global atmospheric ice nuclei distributions and their impacts on climate. *Proceedings of the National Academy of Sciences of the United States of America*, *107*(25), 11217–22. https://doi.org/10.1073/pnas.0910818107

Enertechnix. (2010). *Aerodynamic Lens Advanced concentration technology for superior sensitivity and detection*. Maple Valley.

Formlabs. (2014). *Photopolymer Resin Material Properties*.

Formlabs. (2015). *3D Printing with Desktop Stereolithography: An Introduction for Professional Users*. Retrieved from http://formlabs.com/media/upload/Intro-sla-whitepaper-04.pdf

Friedman, B., Ardon-Dryer, K., Carrasquillo, A., Daumit, K., Boulanger, K., Cross, E., … Cziczo, D. (2013). CCN closure and composition analysis of droplet-forming aerosol. *AIP Conference Proceedings*, *1527*, 832–835. https://doi.org/10.1063/1.4803400

Fuzzi, S., Baltensperger, U., Carslaw, K., Decesari, S., Denier Van Der Gon, H., Facchini, M. C., … Gilardoni, S. (2015). Particulate matter, air quality and climate: Lessons learned and future needs. *Atmospheric Chemistry and Physics*, *15*(14), 8217–8299. https://doi.org/10.5194/acp-15-8217-2015

Hiranuma, N., Möhler, O., Kulkarni, G., Schnaiter, M., Vogt, S., Vochezer, P., … Cziczo, D. J. (2016). Development and characterization of an ice-selecting pumped counterflow virtual impactor (IS-PCVI) to study ice crystal residuals. *Atmospheric Measurement Techniques Discussions*, (April), 1–41. https://doi.org/10.5194/amt-2016-102

Kulkarni, G., Pekour, M., Afchine, A., Murphy, D. M., & Cziczo, D. J. (2011). Comparison of Experimental and Numerical Studies of the Performance Characteristics of a Pumped Counterflow Virtual Impactor. *Aerosol Science and Technology*, *45*(3), 382–392. https://doi.org/10.1080/02786826.2010.539291

Kupiszewski, P., Weingartner, E., Vochezer, P., Schnaiter, M., Bigi, A., Gysel, M., … Baltensperger, U. (2015). The Ice Selective Inlet: A novel technique for exclusive extraction of pristine ice crystals in mixed-phase clouds. *Atmospheric Measurement Techniques*, *8*(8), 3087–3106. https://doi.org/10.5194/amt-8-3087-2015

Lin, H., & Heintzenberg, J. (1995). A theoretical study of the counterflow virtual impactor. *Journal of Aerosol Science*, *26*(6), 903–914. https://doi.org/10.1016/0021-8502(95)00024-7

Lohmann, U., Lüönd, F., & Mahrt, F. (2016). *An Introduction to Clouds* (1st ed.). Cambridge: Cambridge University Press.

Mertes, S., Verheggen, B., Walter, S., Connolly, P. J., Ebert, M., Schneider, J., … Weingartner, E. (2007). Counterflow Virtual Impactor Based Collection of Small Ice Particles in Mixed-Phase Clouds for the Physico-Chemical Characterization of Tropospheric Ice Nuclei: Sampler Description and First Case Study. *Aerosol Science and Technology*, *41*(9), 848–864. https://doi.org/10.1080/02786820701501881

Mesa Laboratories. (2015). *Definer 220 Series User Manual.* https://doi.org/10.1002/ejoc.201200111

Ogren, J. A., Heintzenberg, J., & Charlon, R. J. (1985). In-Situ Sampling of Clouds with a Droplet to Aerosol Converter. *Geophysical Research Letters*, *12*(3), 121–124.

Seifert, P., Ansmann, A., Mattis, I., Wandinger, U., Tesche, M., Engelmann, R., … Haustein, K. (2010). Saharan dust and heterogeneous ice formation: Eleven years of cloud observations at a central European EARLINET site. *Journal of Geophysical Research Atmospheres*, *115*(20), 1–13. https://doi.org/10.1029/2009JD013222

Slowik, J. G., Cziczo, D. J., & Abbatt, J. P. D. (2011). Analysis of cloud condensation nuclei composition and growth kinetics using a pumped counterflow virtual impactor and aerosol mass spectrometer. *Atmospheric Measurement Techniques*, *4*(8), 1677–1688. https://doi.org/10.5194/amt-4-1677-2011

TSI. (2011). *Model 3330 Optical Particle Sizer Spectrometer.*

Figures

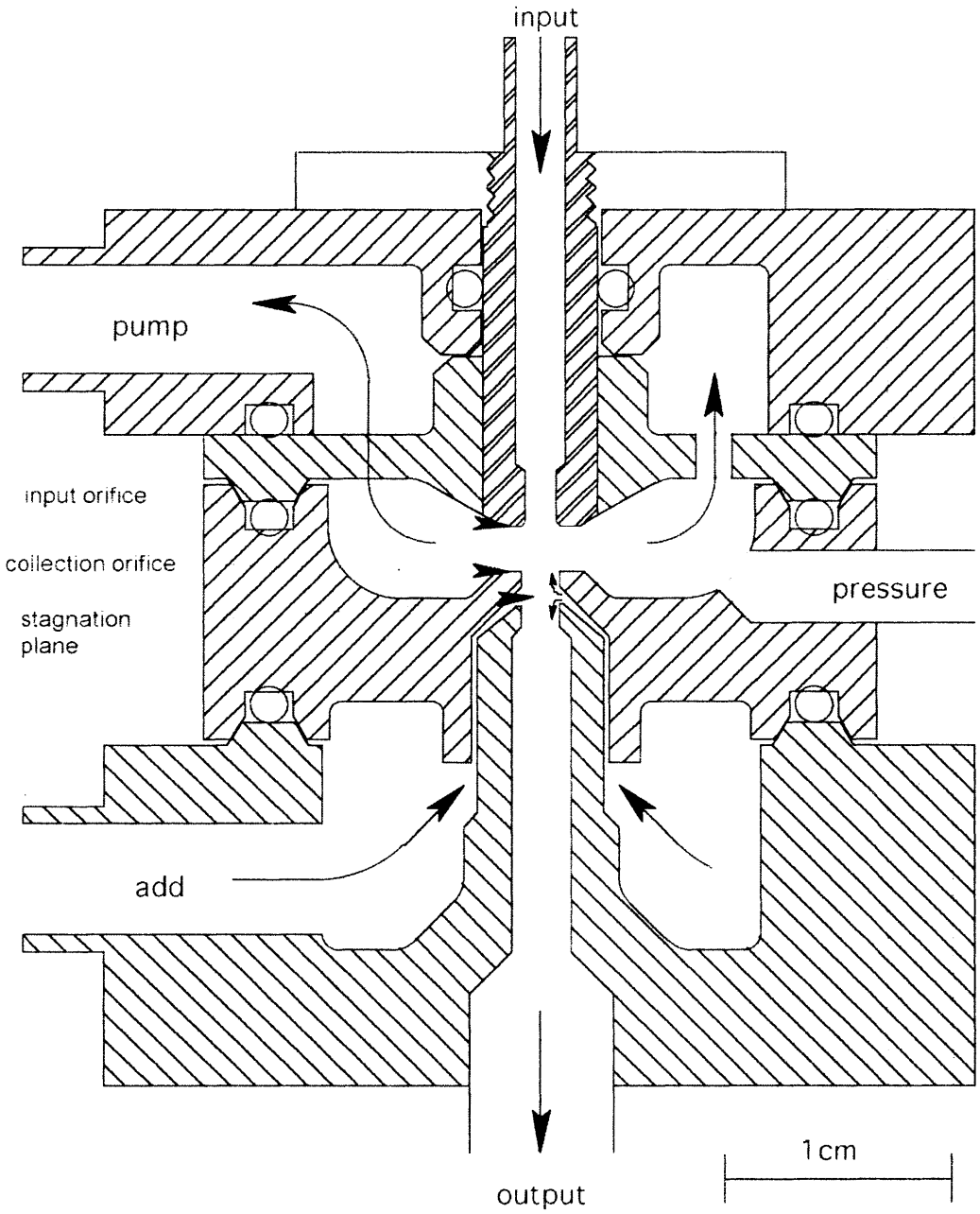

Figure 1 The cross-section of the PCVI adapted from Boulter et al. (2006) shows the locations of the add flow and pump flow with relation to the input and output flow. Particles enter in the input flow and only those with sufficient inertia can cross the stagnation plane to exit through the output flow.

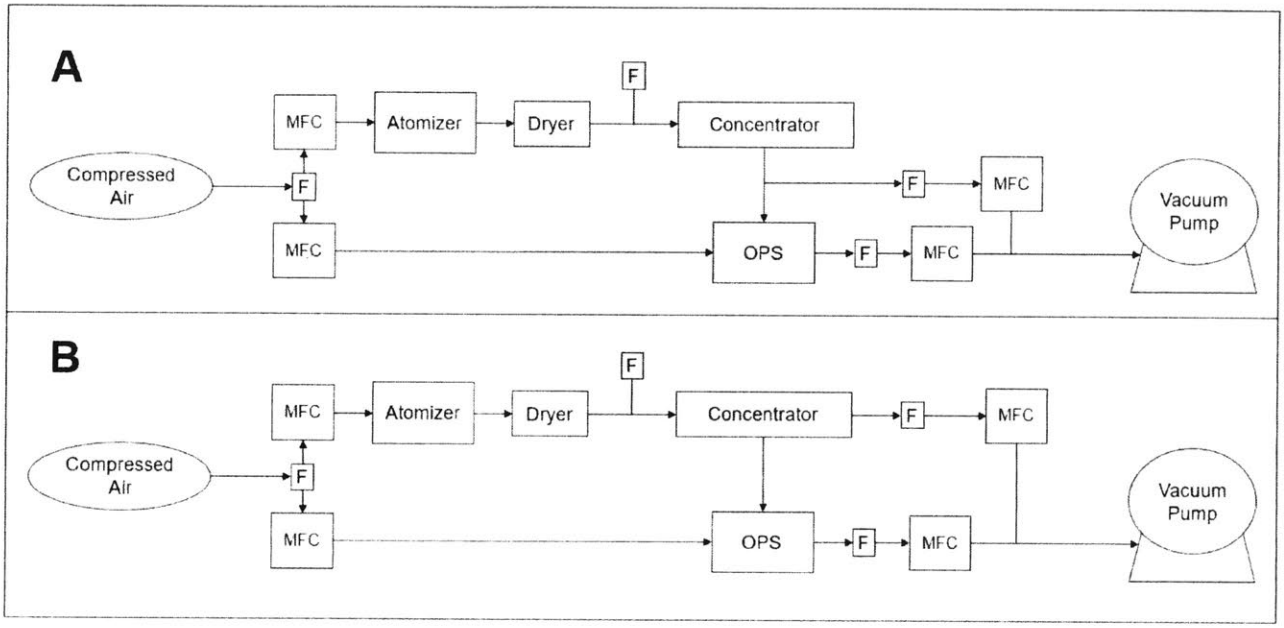

Figure 2 The measurement setup used for studying the concentrator. It incorporates use of filters (F) and mass flow controllers (MFC). **A**: The reference setup for the concentrator involved plugging the pump flow outlet and diluting the output of the concentrator by the same flow ratio that will be used in the sample setup. **B**: The sample setup for the concentrator pulled a constant flow out of the vacuum pump region.

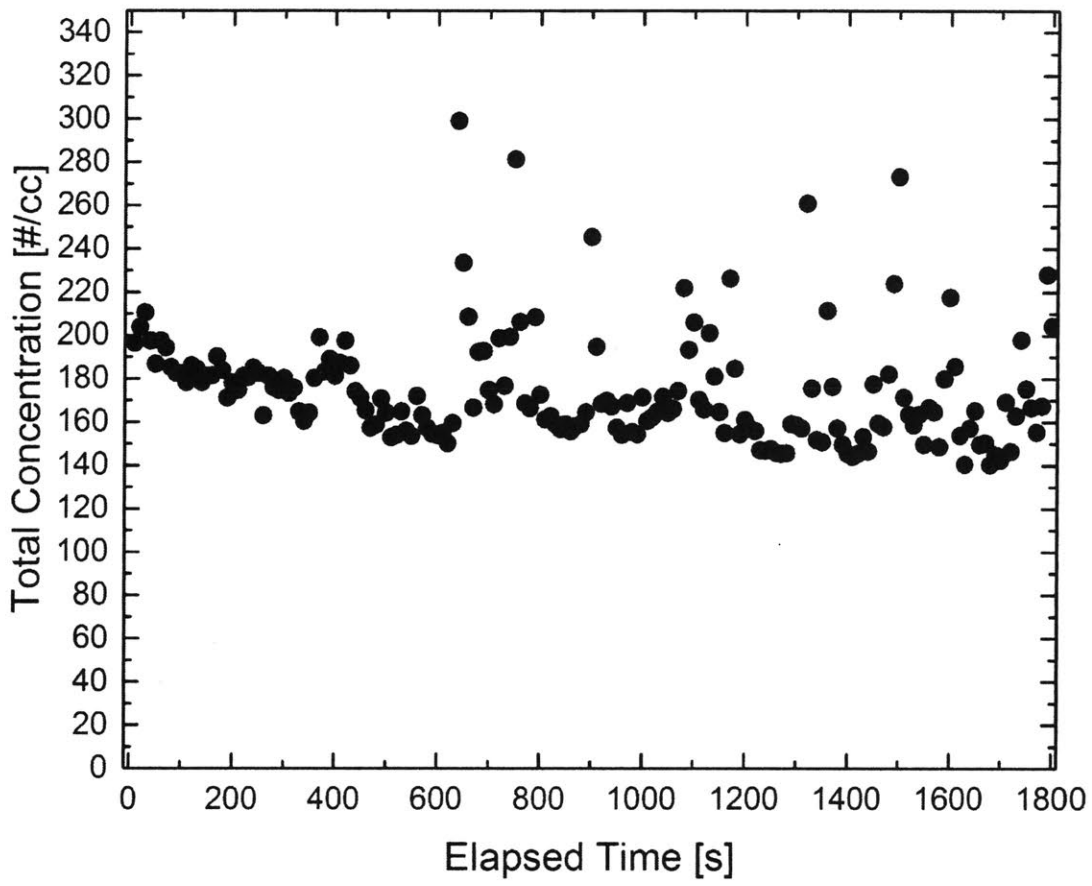

Figure 3 The bubble burst generator was run at 1.114 SLPM for 30 minutes detected with a 1-second resolution and averaged into 10-second bins. The output demonstrated that a 30-minute warm up period is required for generating constant output.

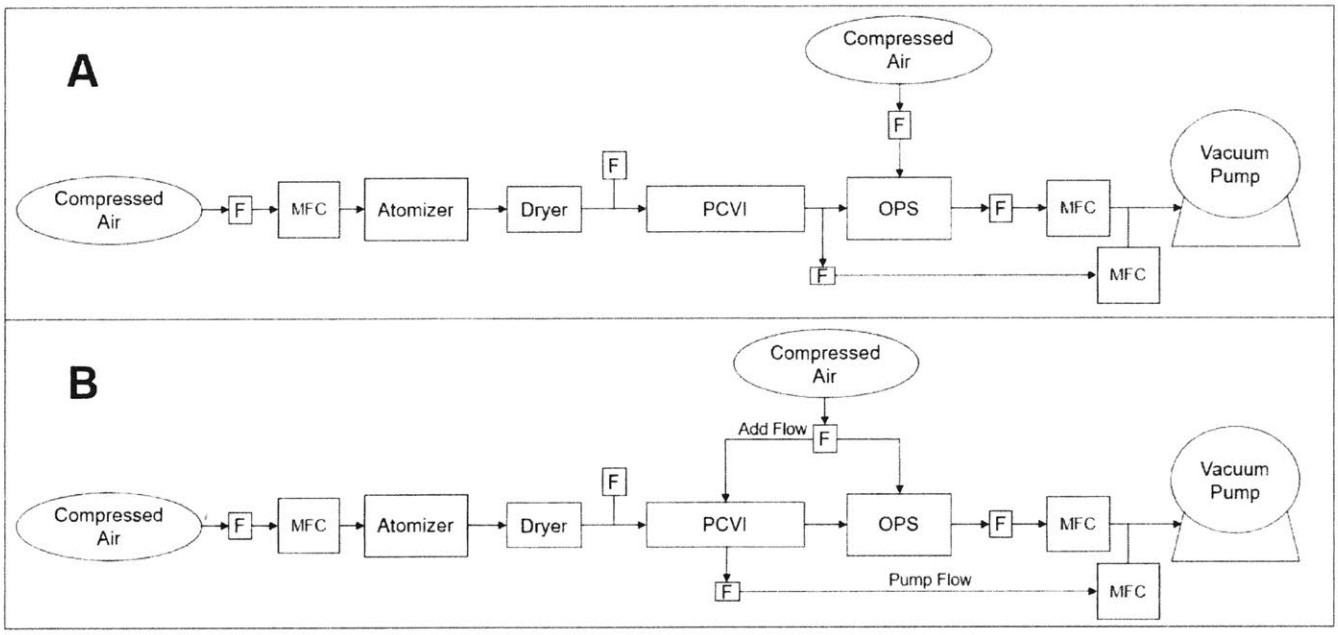

Figure 4 The apparatuses used for studying the PCVI. **A**: The reference setup for the PCVI plugged both the add and pump flows and adjusted a downstream excess flow such that the input flow matched the input flow for the sample test. **B**: The sample setup used MFCs to control a constant add and pump flow.

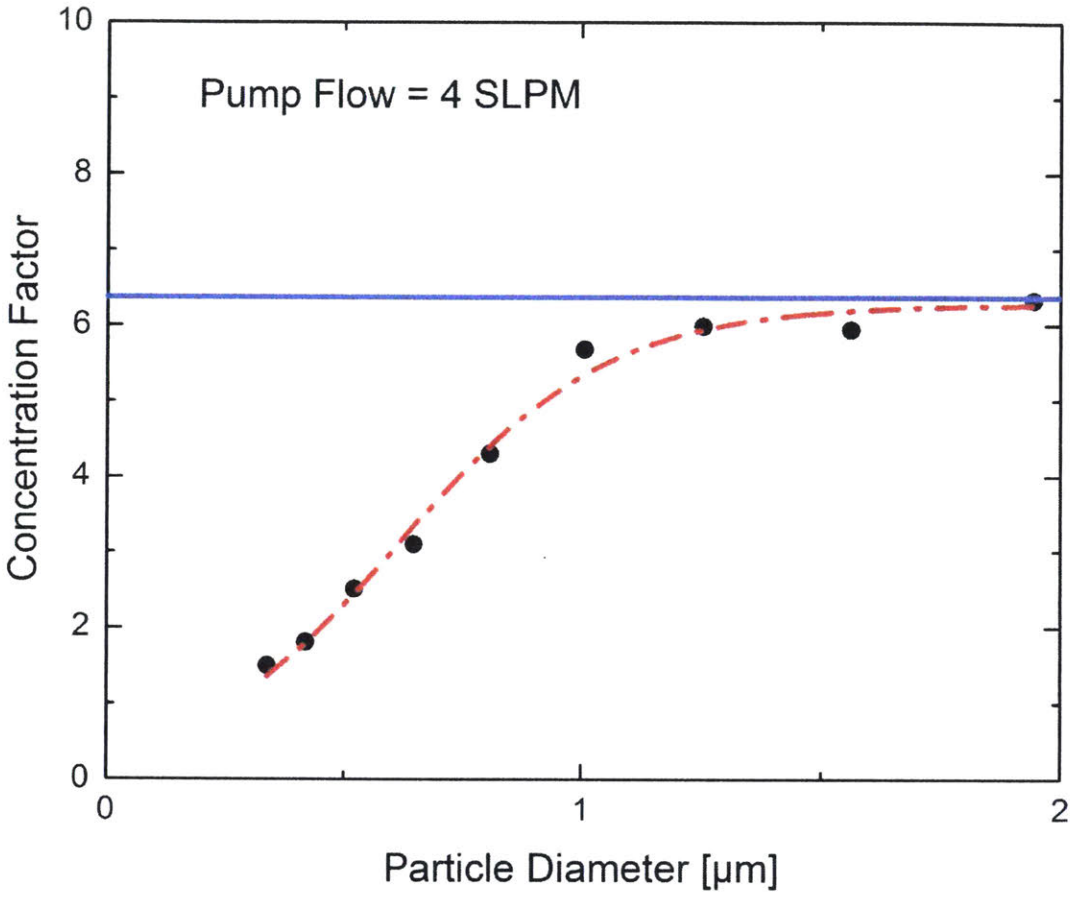

Figure 5 Concentration factor at 4 SLPM pump flow for the industrial concentrator as a function of particle diameter. A sigmoidal curve was fit to the data (red dashed line) and an asymptotic concentration factor was eyeballed for this flow scenario (blue line).

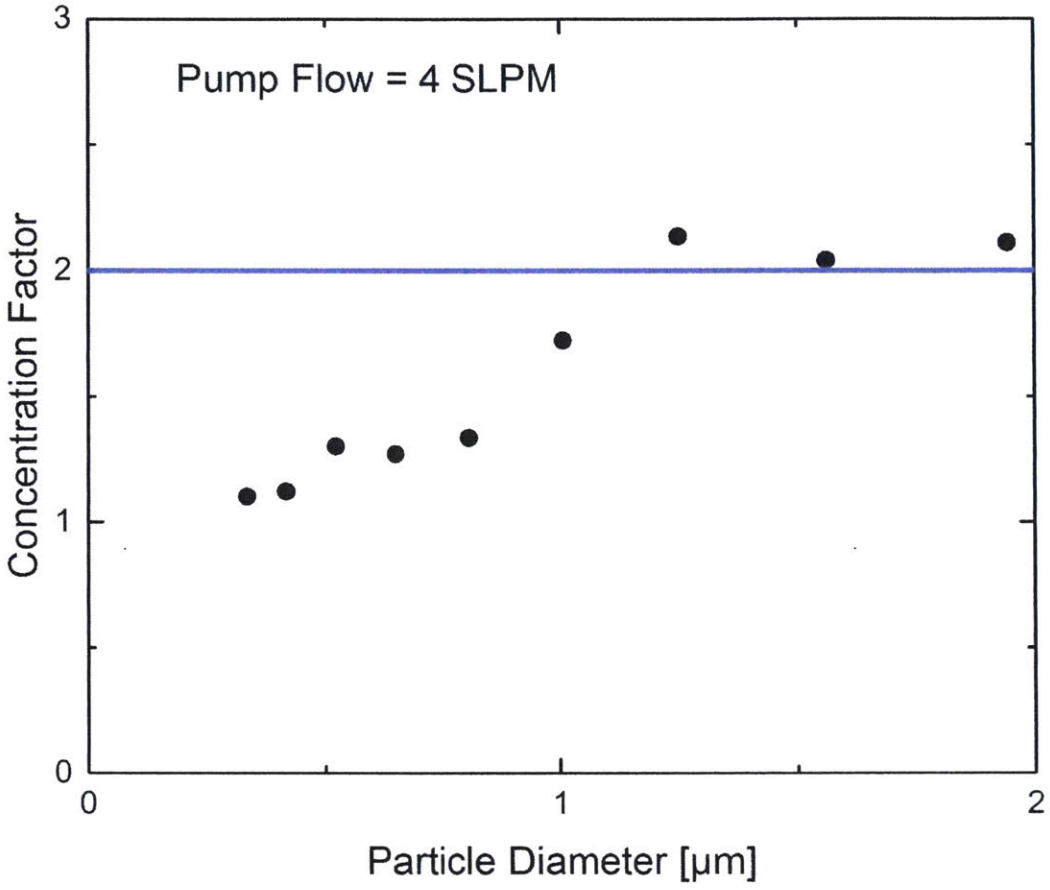

Figure 6 The 4 SLPM pump flow test of the printed concentrator was too noisy for a sigmoidal fit. Instead, the 1-2 μm concentration factors were averaged together to determine the concentration enhancement factor for this flow scenario over this range and is delineated with the blue line.

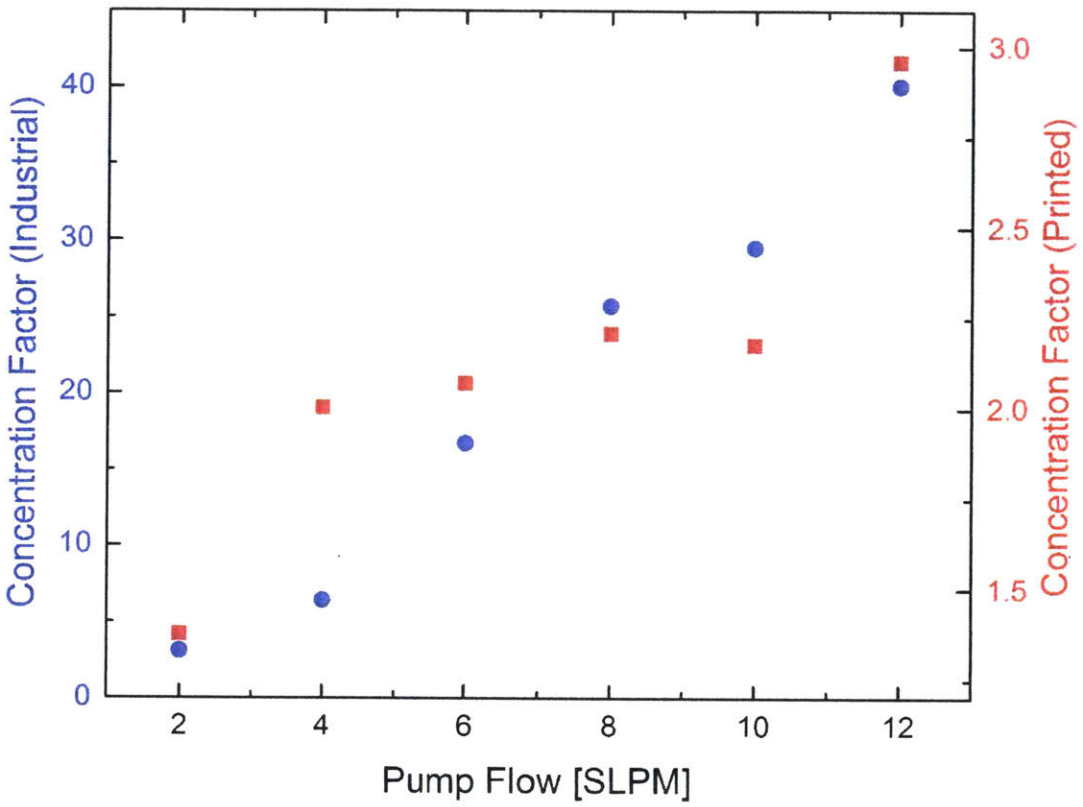

Figure 7 The results of the industrial and printed concentrator test were plotted together on separate axes. The blue dots and axis refer to the results of the industrial concentrator; the printed concentrator is represented in red.

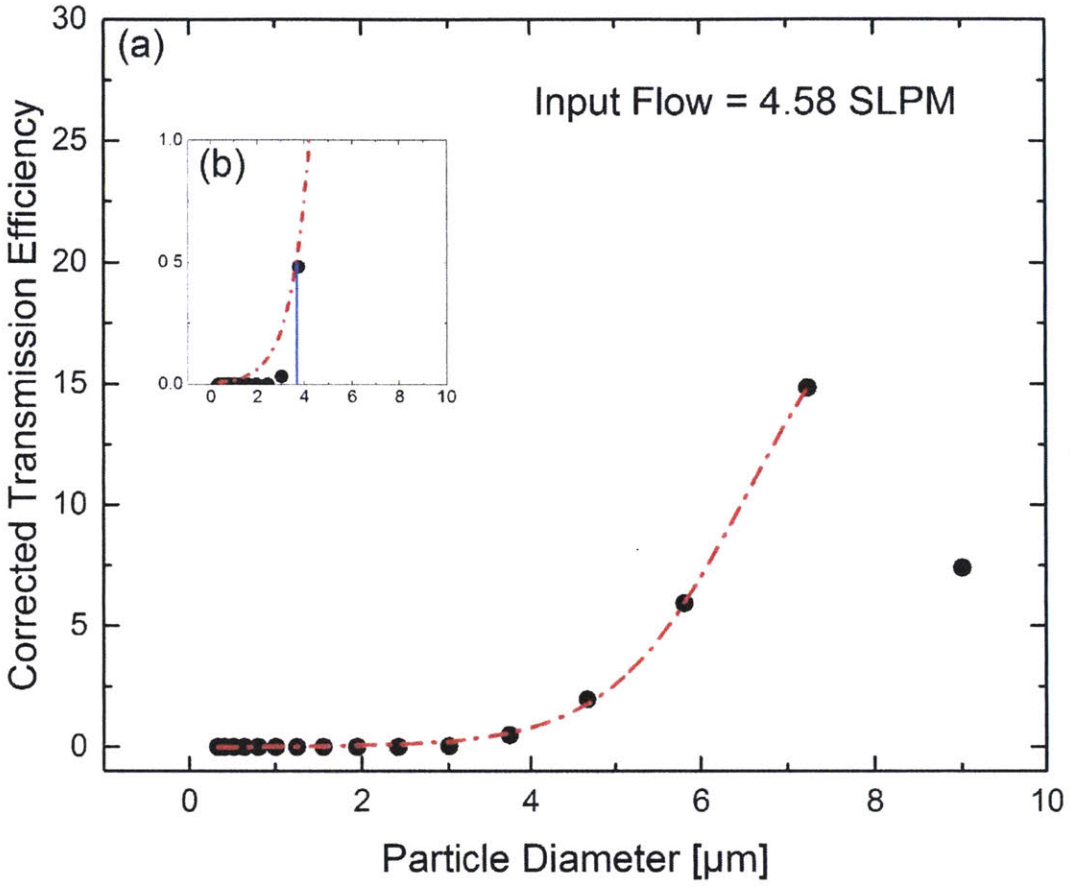

Figure 8 **A:** The transmission curve for the industrial PCVI using an input flow of 4.58 SLPM. **B:** The D50 was found to be approximately 3.7 µm.

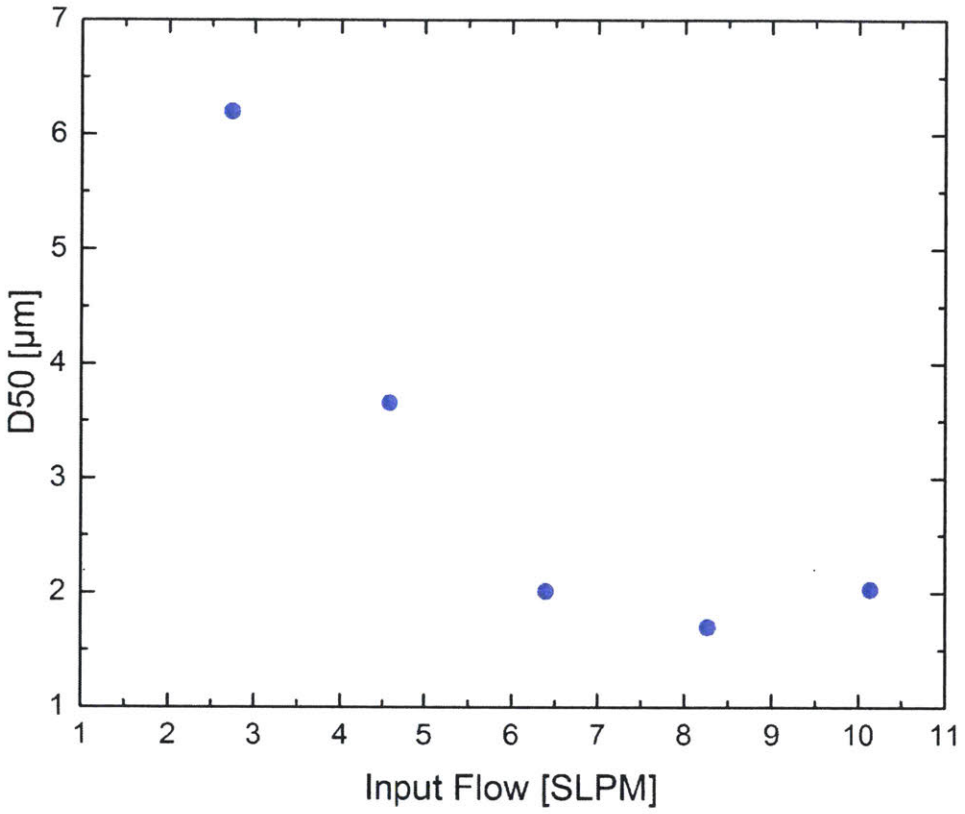

Figure 9 The D50 for varying input flows into the industrial concentrator. For these tests, add flow and sample flow were held constant.

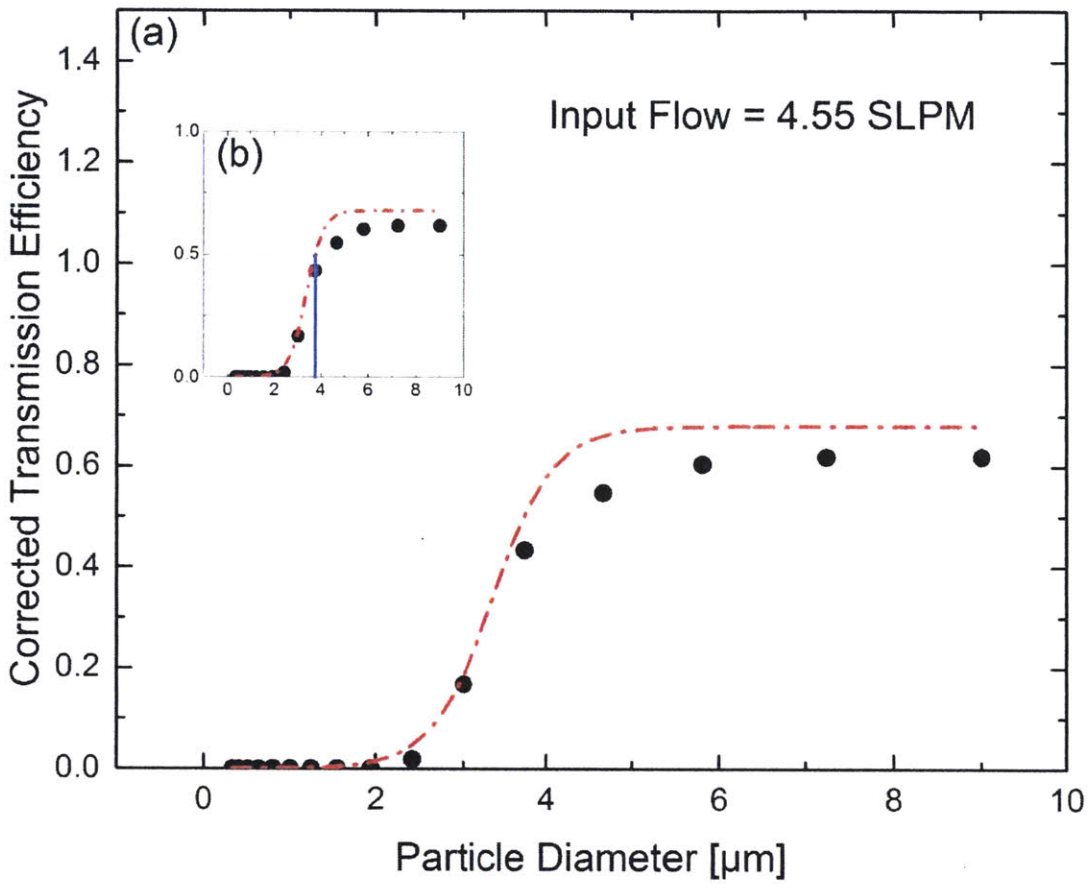

Figure 10 **A:** The transmission curve for the printed PCVI using an input flow of 4.55 SLPM. **B:** The D50 was found to be approximately 3.7 µm.

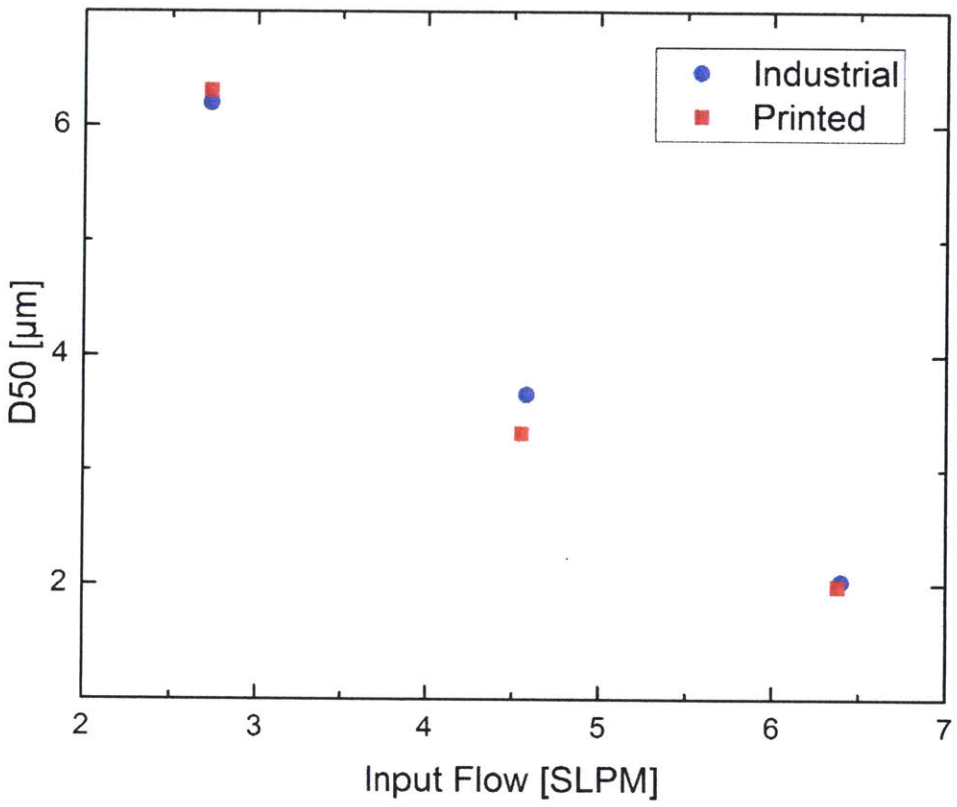

Figure 11 Comparison of D50 values for the industrial and printed PCVI as a function of input flow in their overlapping range of functionality from pump flows between 5 and 7.5 SLPM.

Tables

TABLE 1 The industrial and printed concentrators were compared over the range of functional pump flows for the printed concentrator.

Pump Flow [SLPM]	Concentration Enhancement Factor	
	Industrial Concentrator	Printed Concentrator
2	3.1	1.4
4	6.4	2.0
6	16.7	2.1
8	25.7	2.2
10	29.5	2.2
12	40.1	3.0

TABLE 2 The industrial PCVI was tested with five distinct flow scenarios in standard liters per minute (SLPM). The resulting D50 values follow the theoretical decrease with increased input flow until 8 SLPM.

Input Flow [SLPM]	D_{50} [μm]
2.73	6.20
4.58	3.66
6.40	2.03
8.27	1.71
10.14	2.05

TABLE 3 Both PCVIs were compared to the experimental and modelled results from the Kulkarni et al. (2011) experiments.

Input Flow [LPM]	50% Cut Size [μm]			
	Printed PCVI	Industrial PCVI	Kulkarni et al. (2011)	
			Experimental	CFD Model
11.97	1.54	2.02	2.24	2.18
9.64	1.74	-	2.68	2.52
9.20	1.81	-	3.09	3.10
8.60	3.89	-	3.77	4.05
6.90	2.02	2.69	3.21	2.81
6.88	2.71	-	3.42	3.45
6.78	2.23	-	3.40	3.40
6.70	3.89	-	4.05	4.30
6.60	4.82	4.48	4.81	4.80
6.50	4.35	-	4.65	4.78

Appendix

A. CONCENTRATOR CHARACTERIZATIONS

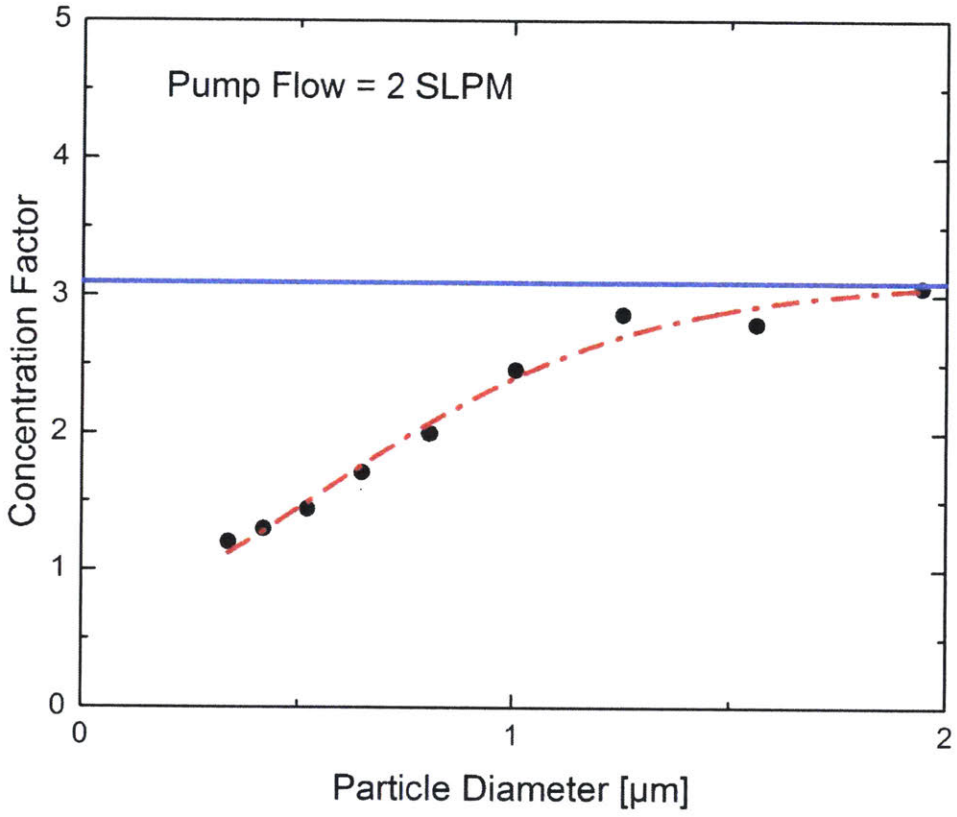

Figure A1 The industrial concentrator with a pump flow of 2 SLPM had a concentration enhancement factor of approximately 3.1.

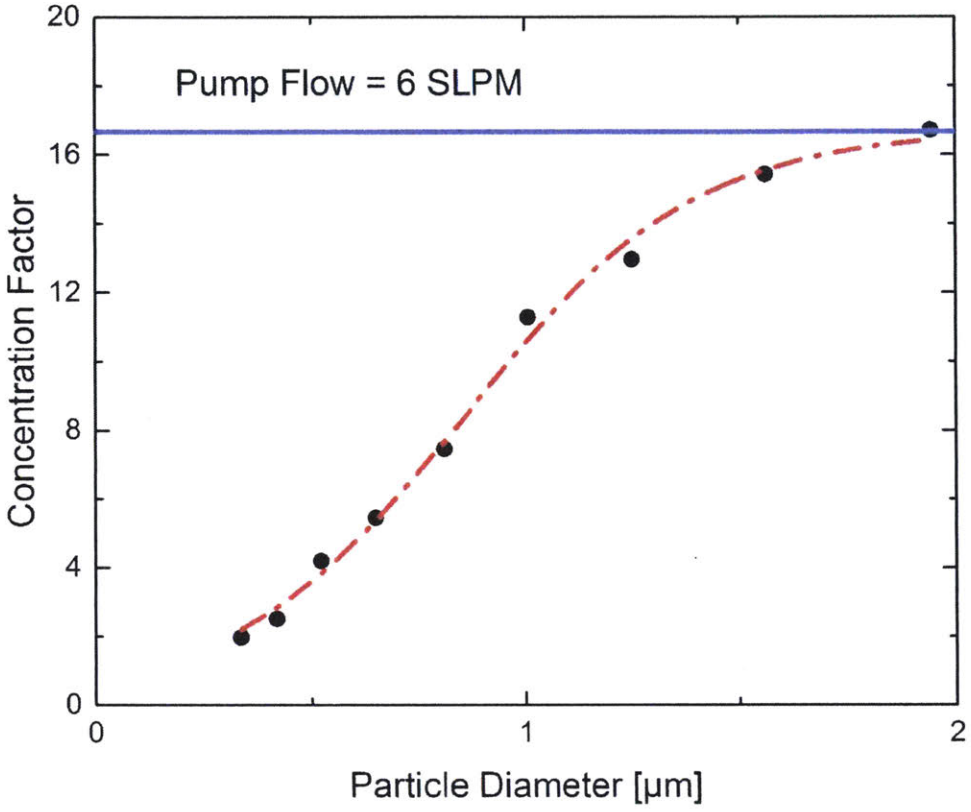

Figure A2 The industrial concentrator with a pump flow of 6 SLPM had a concentration enhancement factor of approximately 16.7.

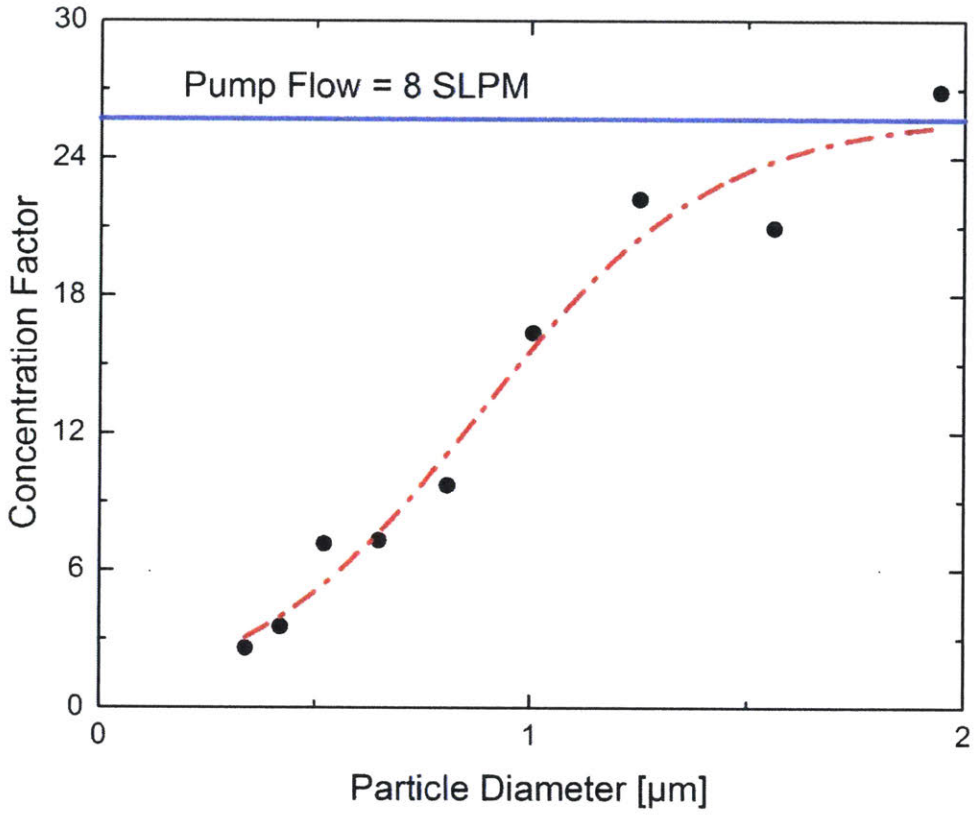

Figure A3 The industrial concentrator with a pump flow of 8 SLPM had a concentration enhancement factor of approximately 25.7.

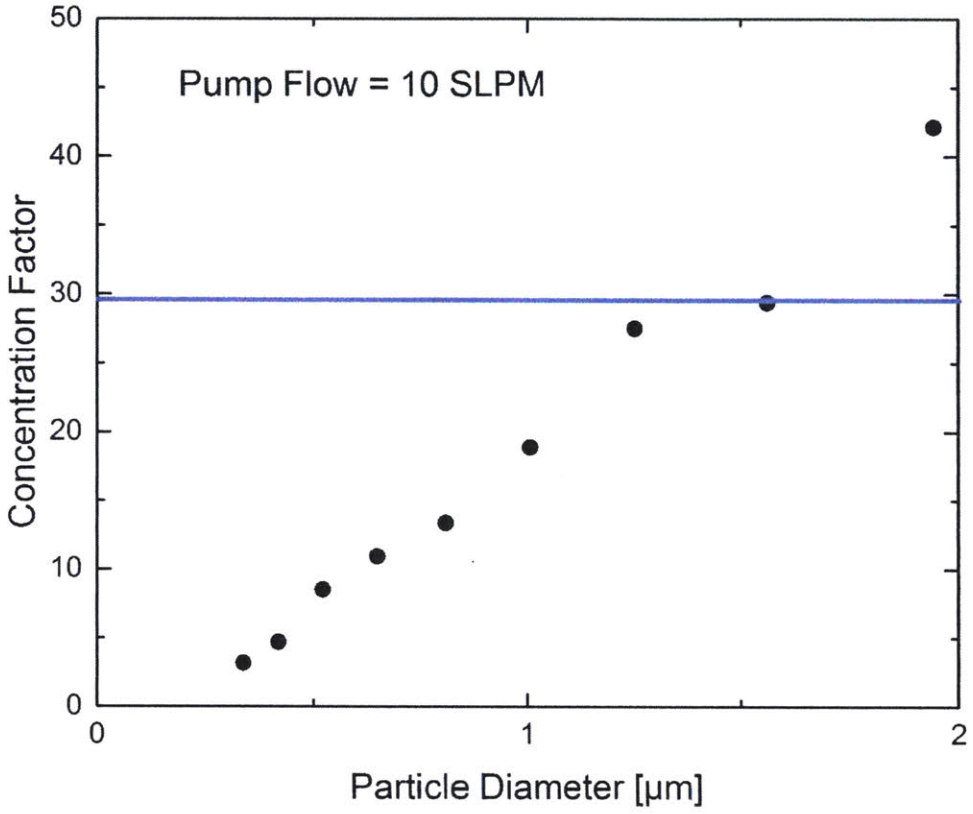

Figure A4 The industrial concentrator with a pump flow of 10 SLPM had a concentration enhancement factor of approximately 29.5.

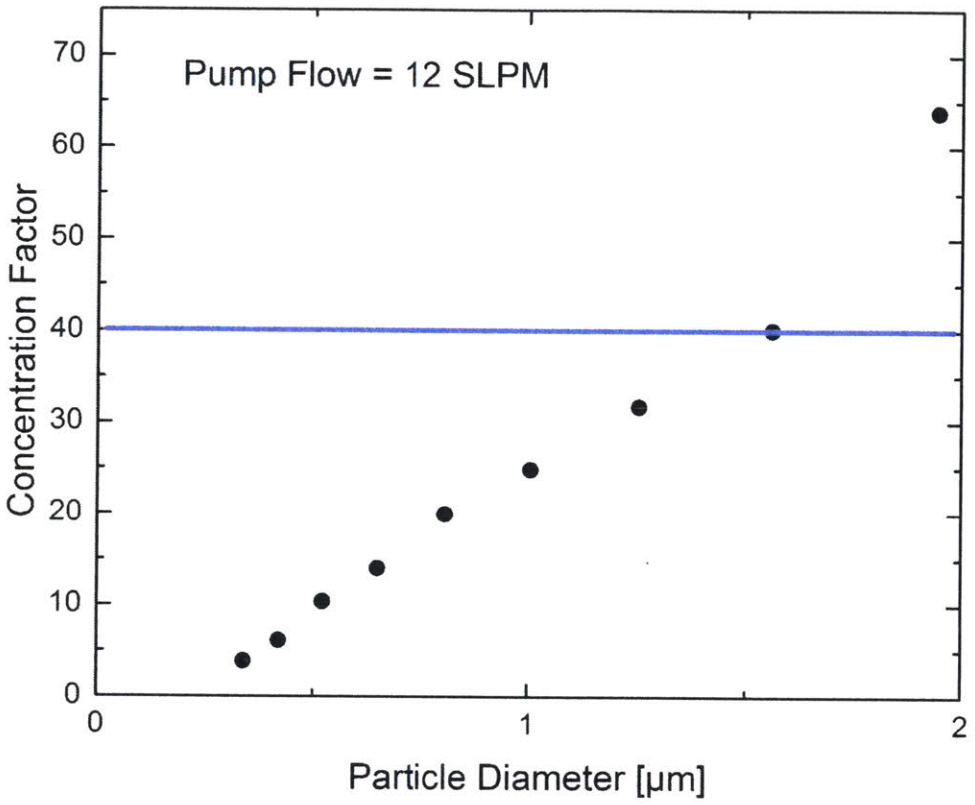

Figure A5 The industrial concentrator with a pump flow of 12 SLPM had a concentration enhancement factor of approximately 40.1.

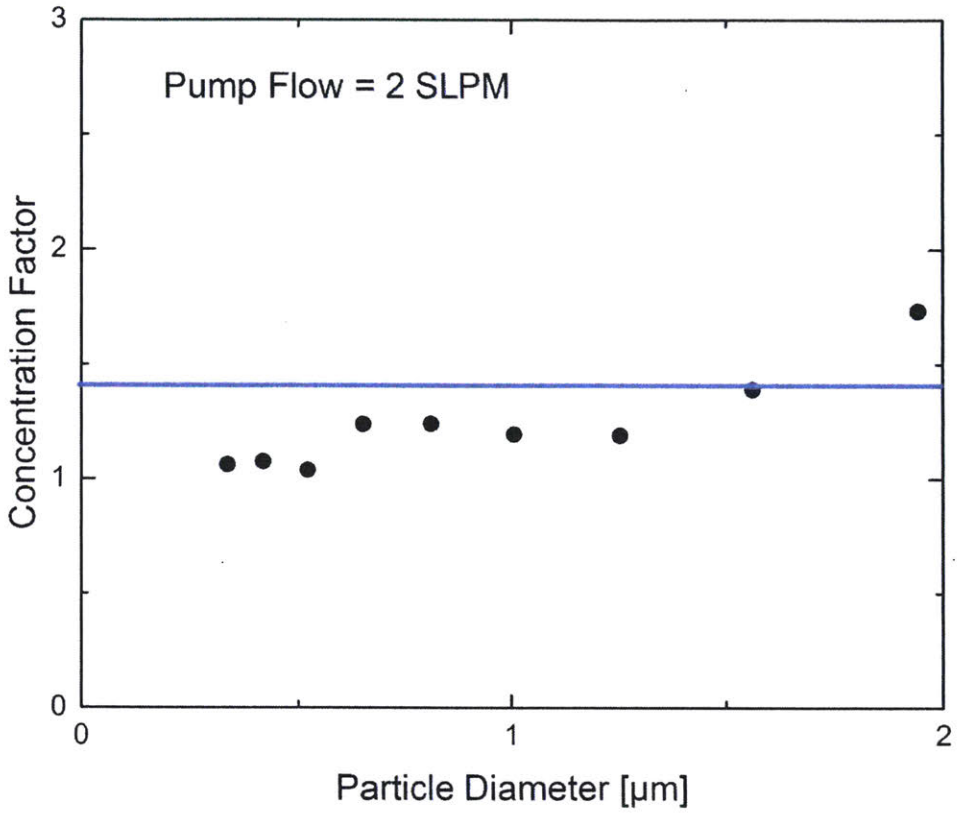

Figure A6 The printed concentrator with a pump flow of 2 SLPM had a concentration enhancement factor of approximately 1.4.

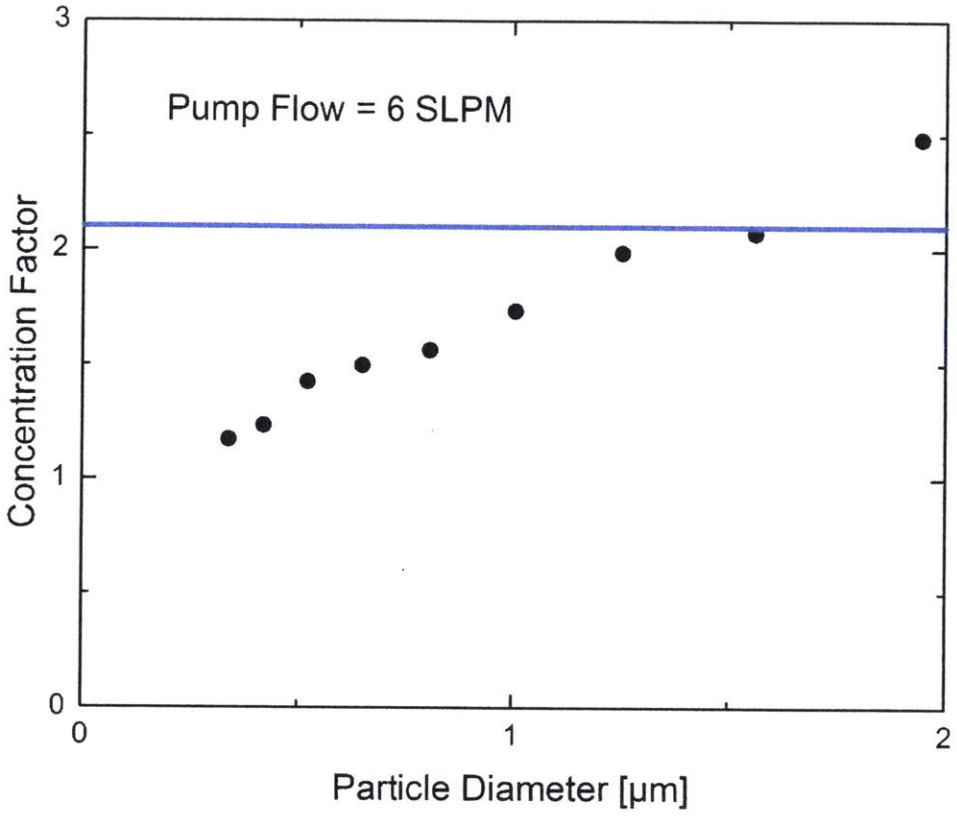

Figure A7 The printed concentrator with a pump flow of 6 SLPM had a concentration enhancement factor of approximately 2.1.

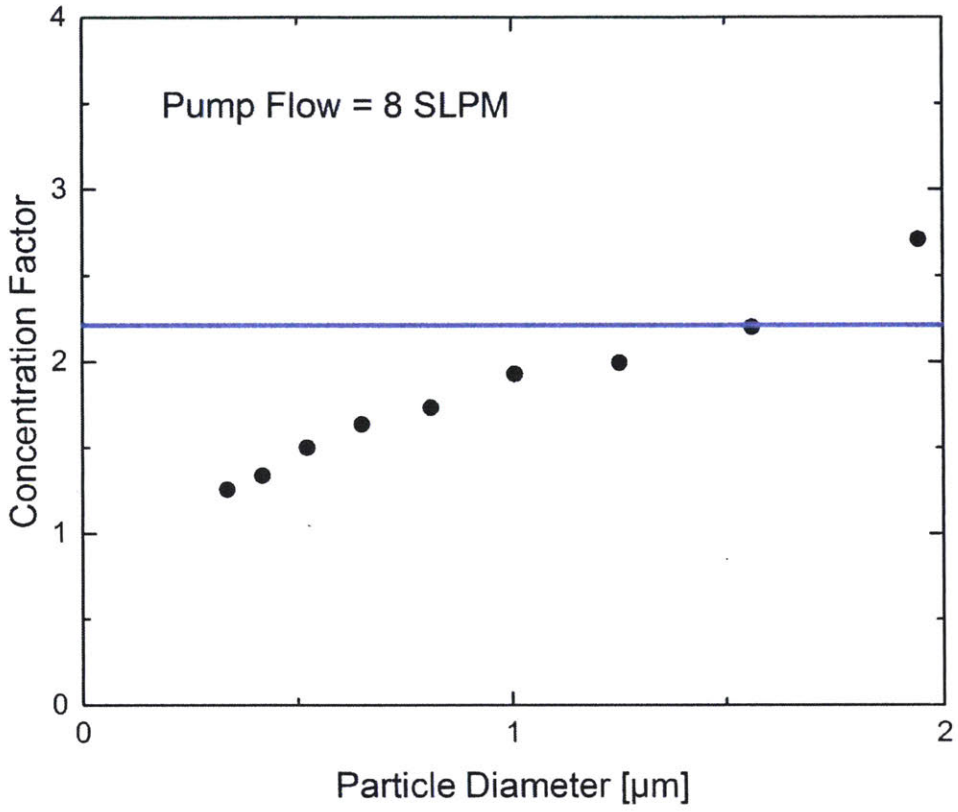

Figure A8 The printed concentrator with a pump flow of 8 SLPM had a concentration enhancement factor of approximately 2.2.

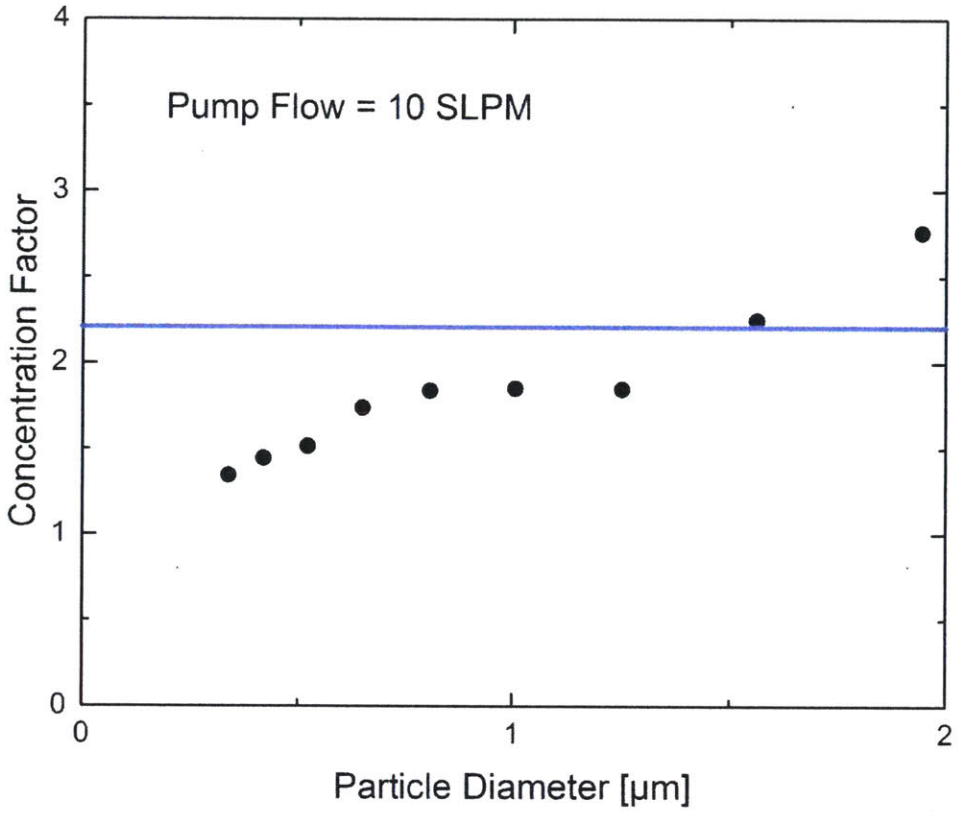

Figure A9 The printed concentrator with a pump flow of 10 SLPM had a concentration enhancement factor of approximately 2.2.

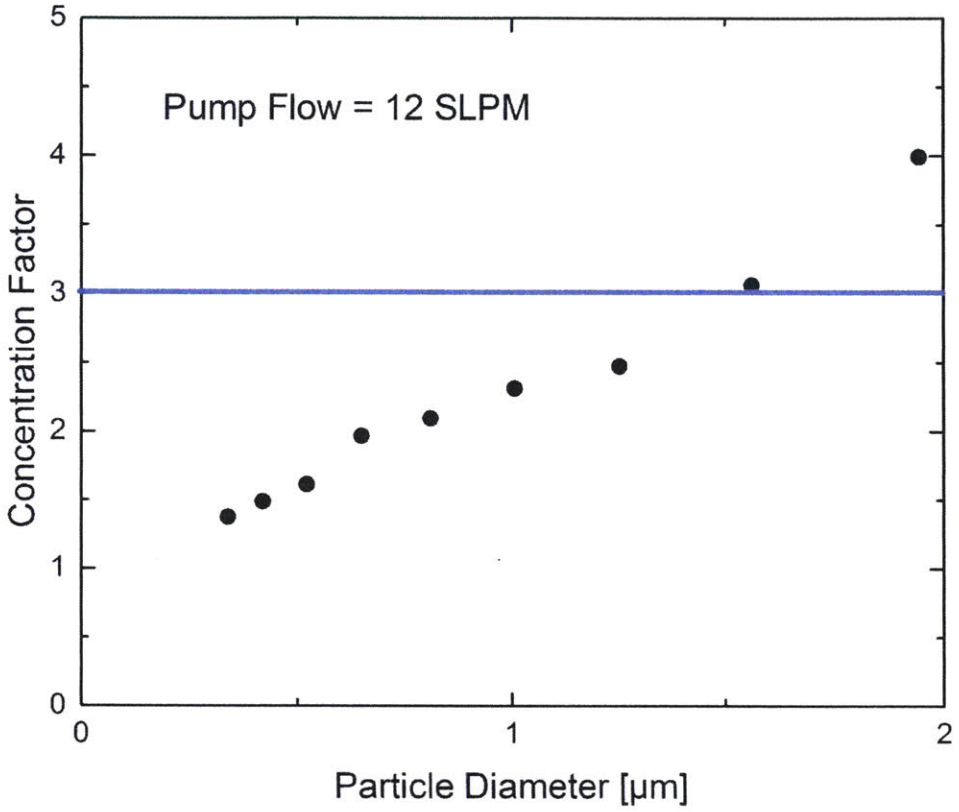

Figure A10 The printed concentrator with a pump flow of 12 SLPM had a concentration enhancement factor of approximately 3.0.

B. INDUSTRIAL PCVI CHARACTERIZATIONS

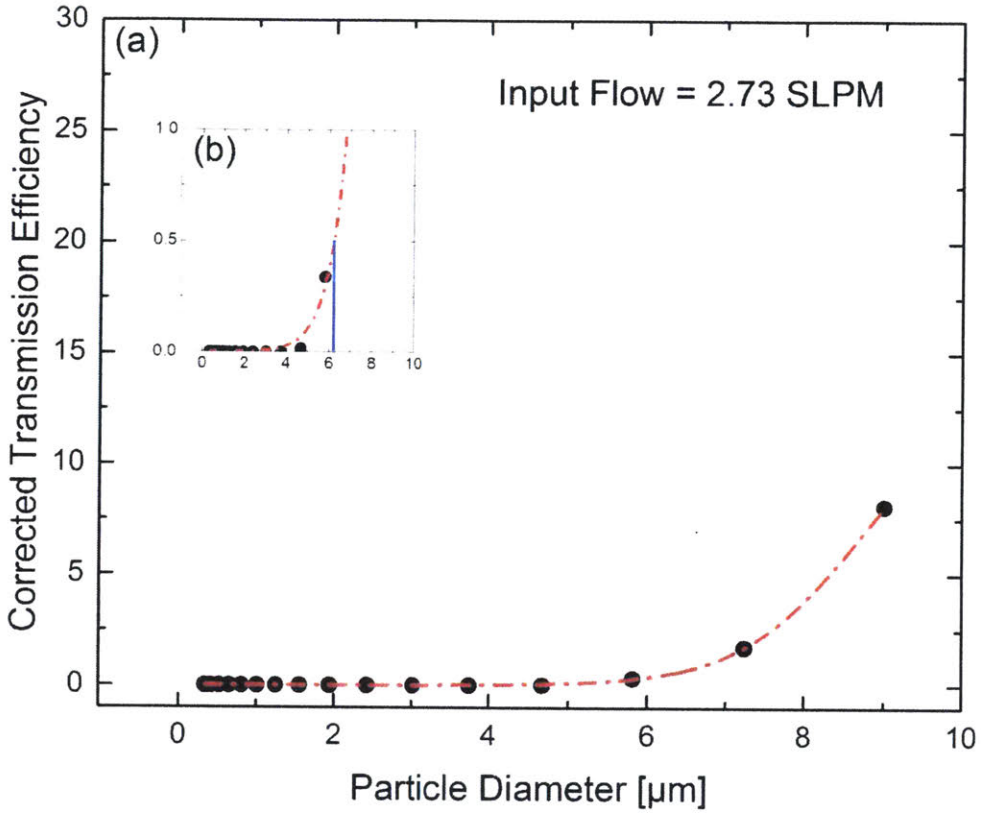

Figure B1 **A:** The transmission efficiency for the industrial PCVI at an input flow of 2.73 SLPM. **B:** The industrial PCVI with an input flow of 2.73 SLPM had a D50 value of approximately 6.2 μm.

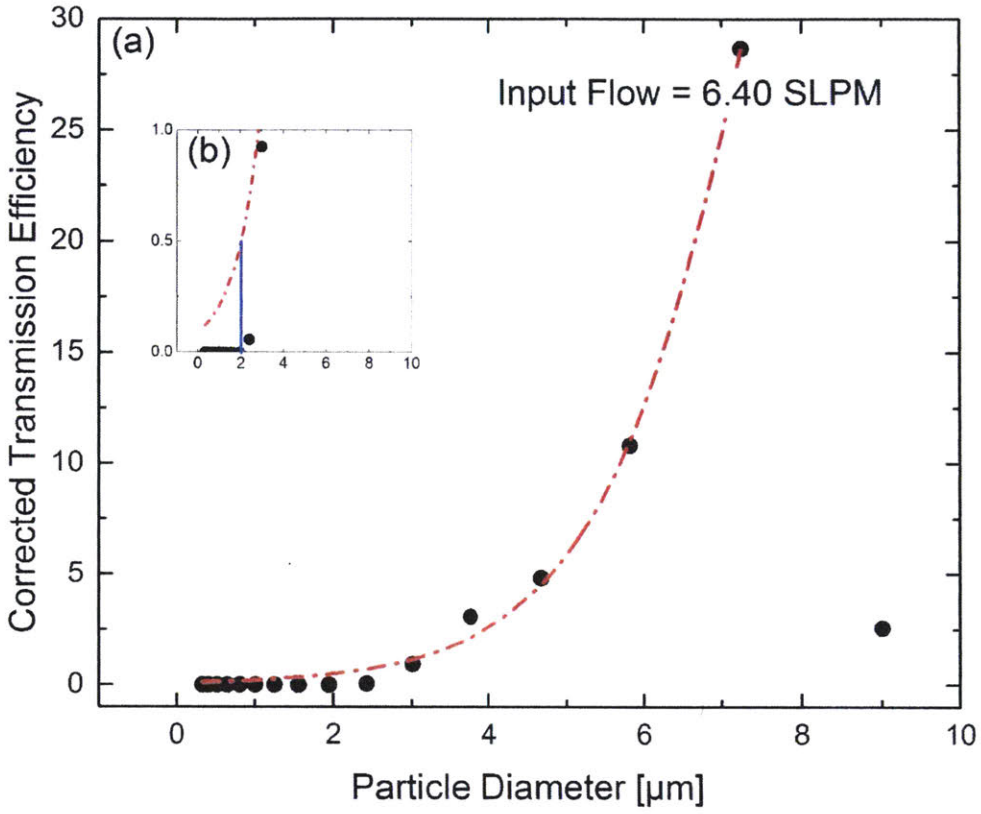

Figure B2 **A:** The transmission efficiency for the industrial PCVI at an input flow of 6.40 SLPM. **B:** The industrial PCVI with an input flow of 6.40 SLPM had a D50 value of approximately 2.0 µm.

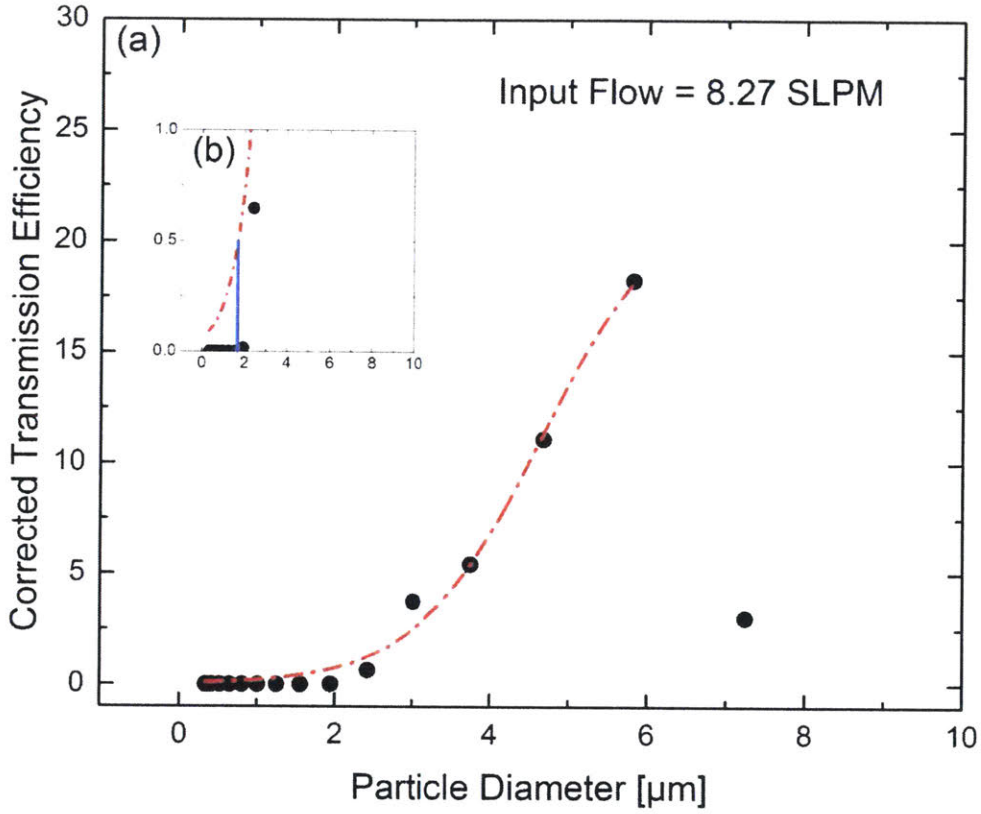

Figure B3 **A:** The transmission efficiency for the industrial PCVI at an input flow of 8.27 SLPM. **B:** The industrial PCVI with an input flow of 8.27 SLPM had a D50 value of approximately 1.7 µm.

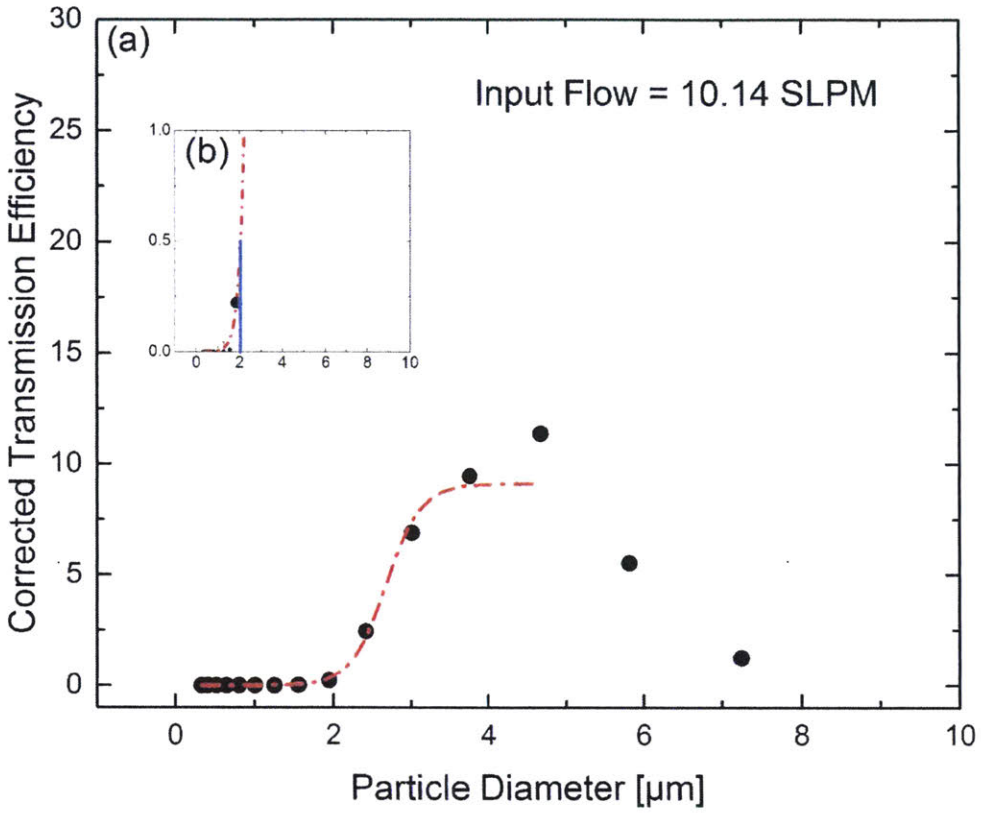

Figure B4 **A:** The transmission efficiency for the industrial PCVI at an input flow of 10.14 SLPM. **B:** The industrial PCVI with an input flow of 10.14 SLPM had a D50 value of approximately 2.0 μm.

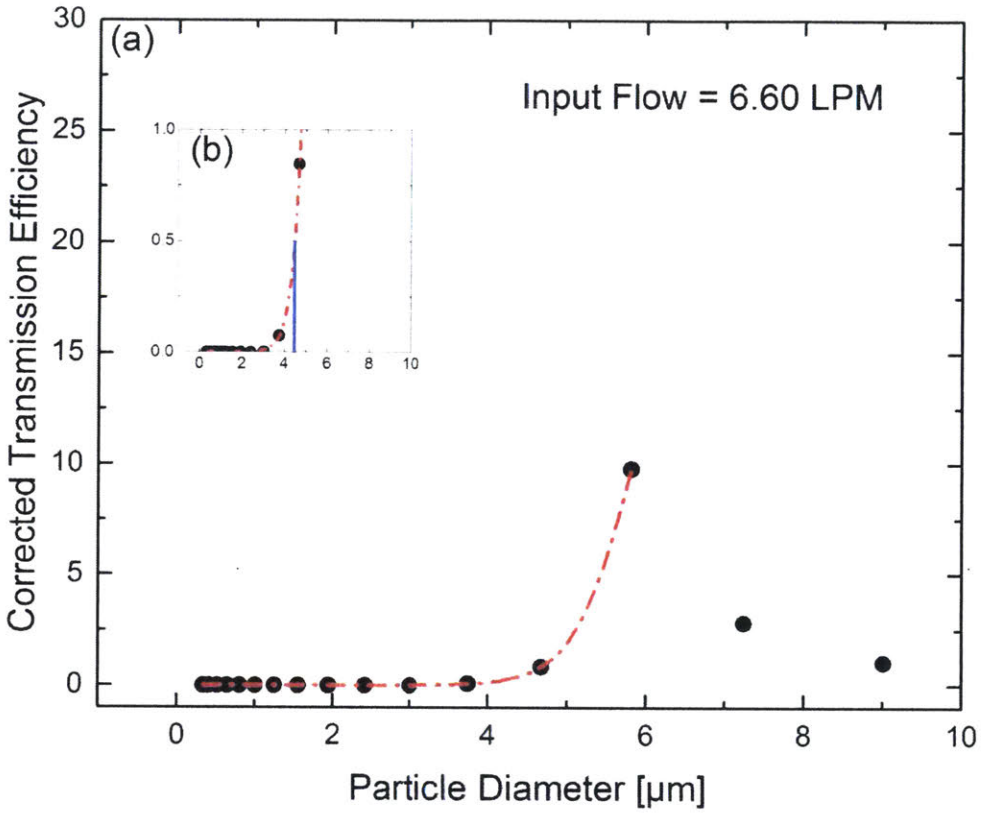

Figure B5 **A:** The transmission efficiency for the industrial PCVI at an input flow of 6.60 LPM. **B:** The industrial PCVI with an input flow of 6.60 LPM had a D50 value of approximately 4.5 µm.

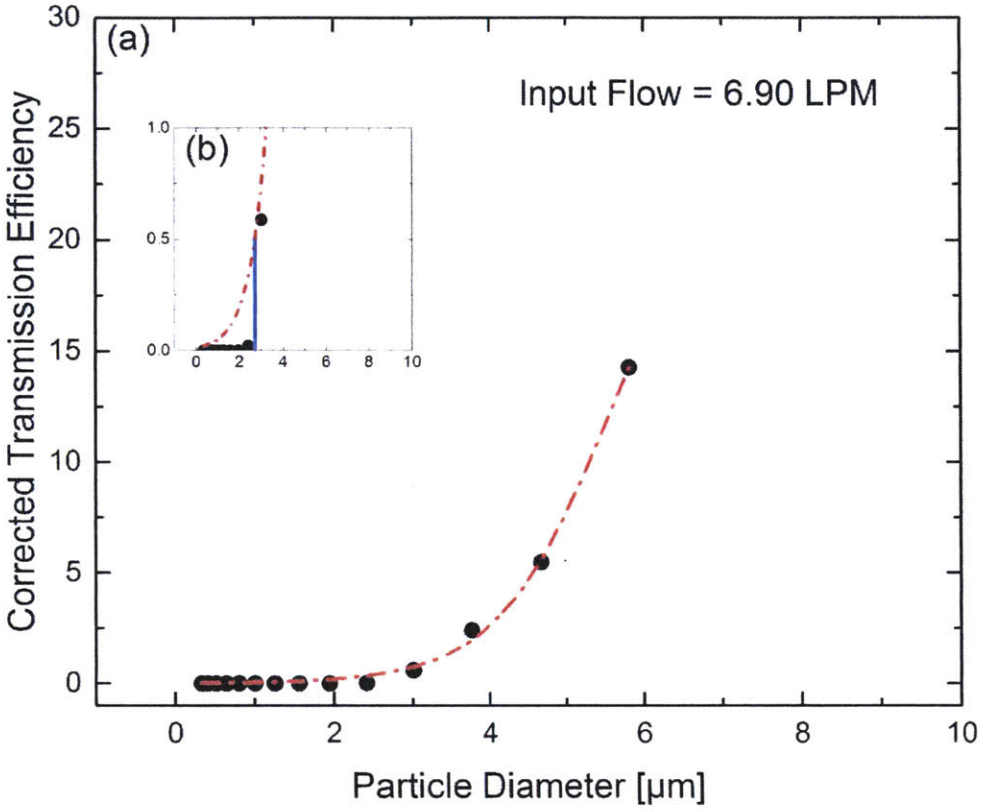

Figure B6 **A:** The transmission efficiency for the industrial PCVI at an input flow of 6.90 LPM. **B:** The industrial PCVI with an input flow of 6.90 LPM had a D50 value of approximately 2.7 µm.

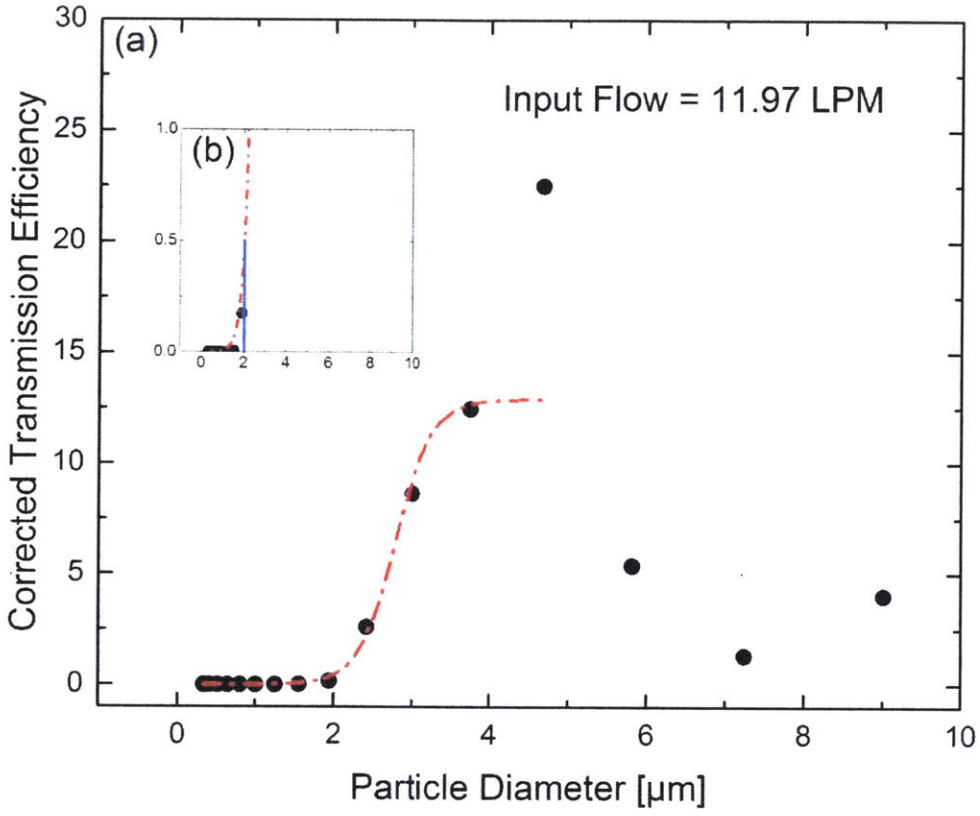

Figure B7 **A:** The transmission efficiency for the industrial PCVI at an input flow of 11.97 LPM. **B:** The industrial PCVI with an input flow of 11.97 LPM had a D50 value of approximately 2.0 µm.

C. PRINTED PCVI CHARACTERIZATIONS

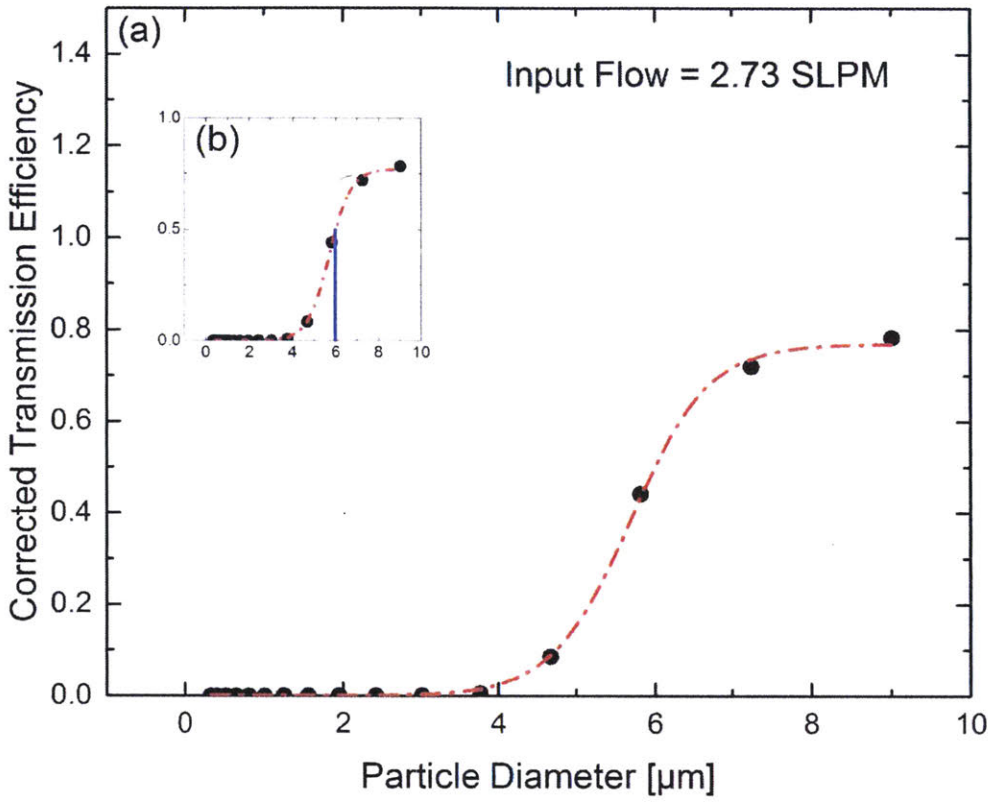

Figure C1 **A:** The transmission efficiency for the printed PCVI at an input flow of 2.73 SLPM. **B:** The printed PCVI with an input flow of 2.73 SLPM had a D50 value of approximately 6.0 μm.

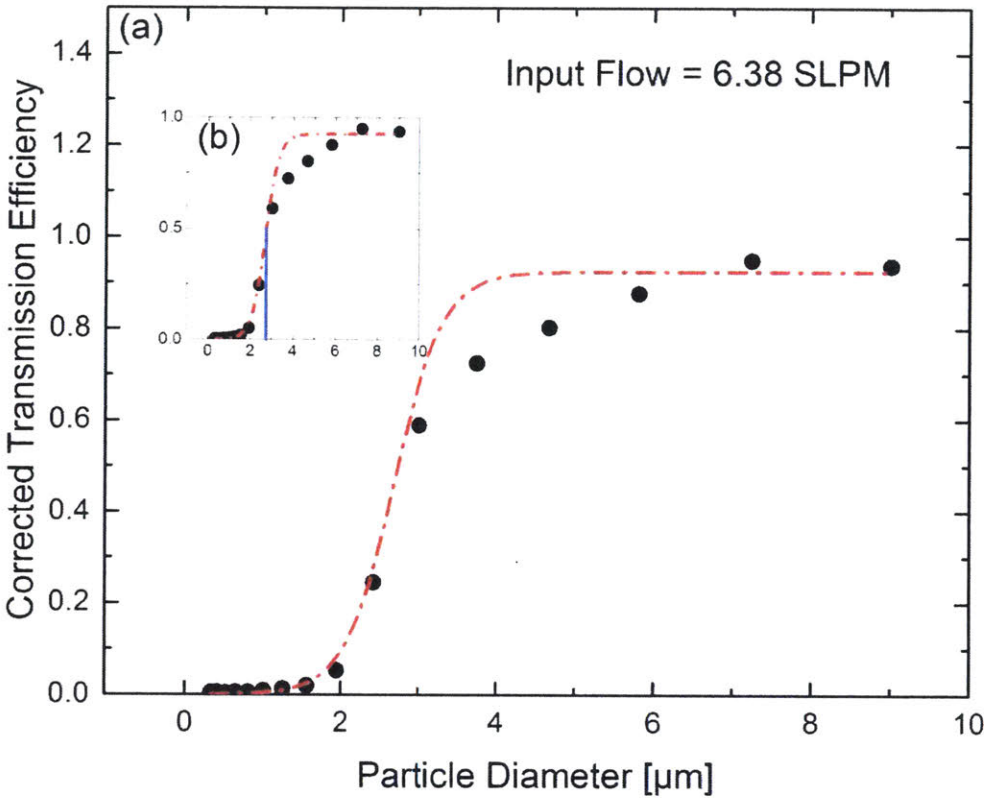

Figure C2 **A:** The transmission efficiency for the printed PCVI at an input flow of 6.38 SLPM. **B:** The printed PCVI with an input flow of 6.38 SLPM had a D50 value of approximately 2.7 µm.

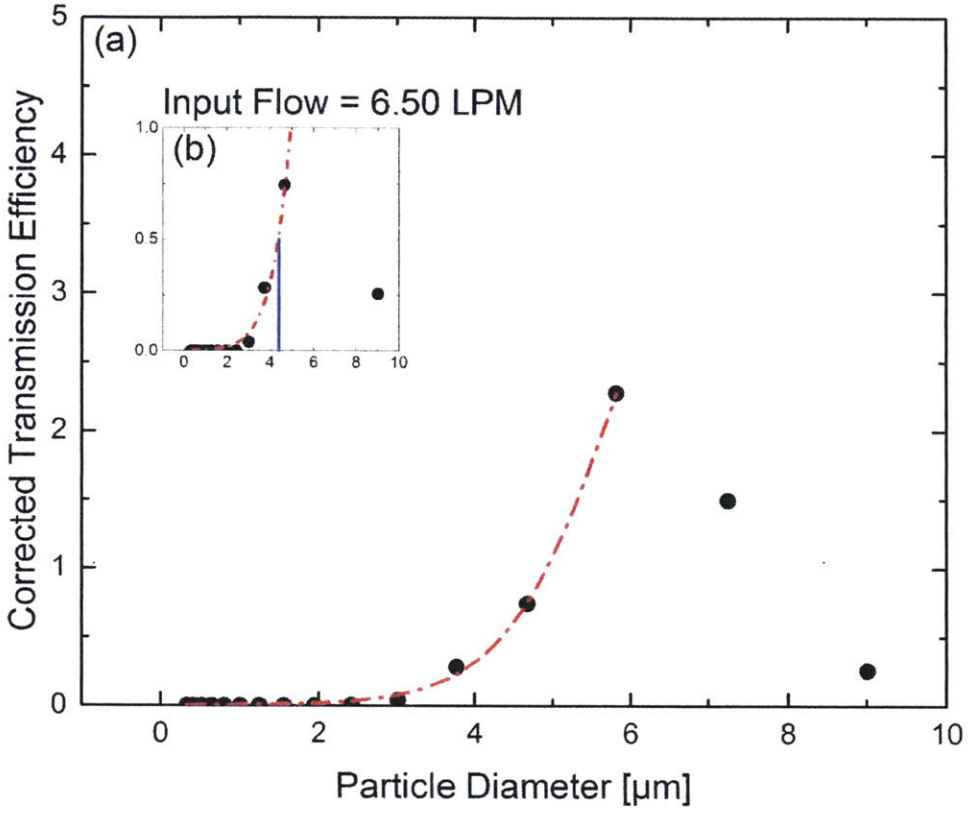

Figure C3 **A:** The transmission efficiency for the printed PCVI at an input flow of 6.50 LPM. **B:** The printed PCVI with an input flow of 6.50 LPM had a D50 value of approximately 4.4 μm.

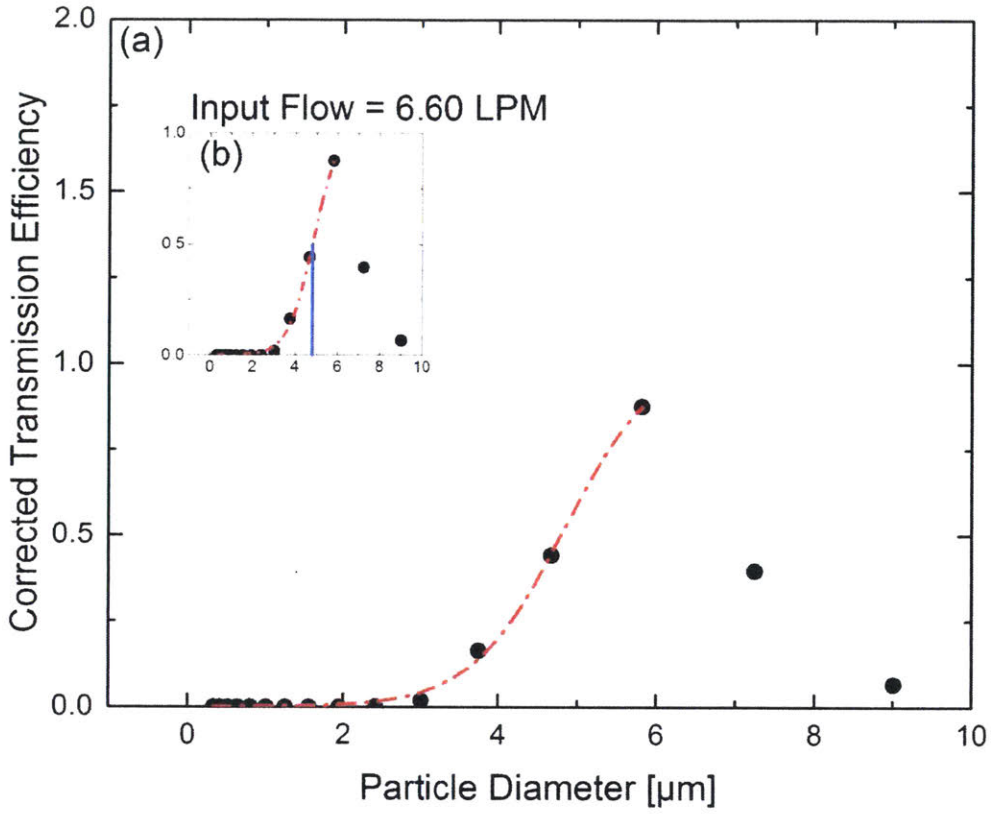

Figure C4 **A:** The transmission efficiency for the printed PCVI at an input flow of 6.60 LPM. **B:** The printed PCVI with an input flow of 6.60 LPM had a D50 value of approximately 4.8 µm.

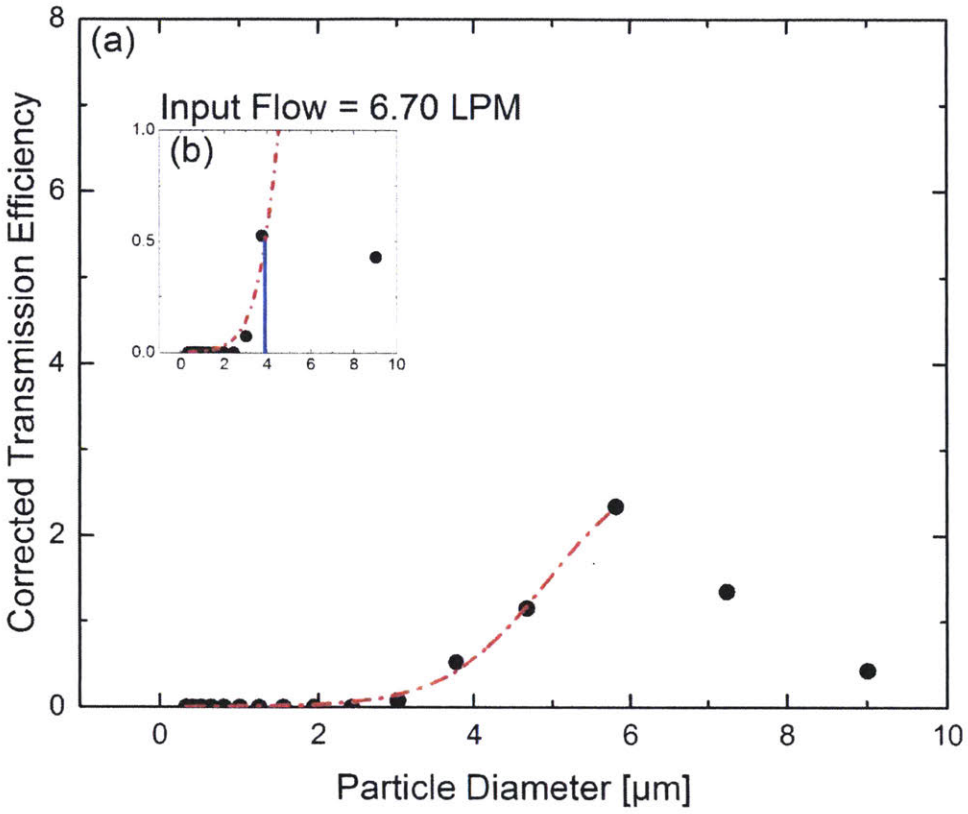

Figure C5 **A:** The transmission efficiency for the printed PCVI at an input flow of 6.70 LPM. **B:** The printed PCVI with an input flow of 6.70 LPM had a D50 value of approximately 3.9 μm.

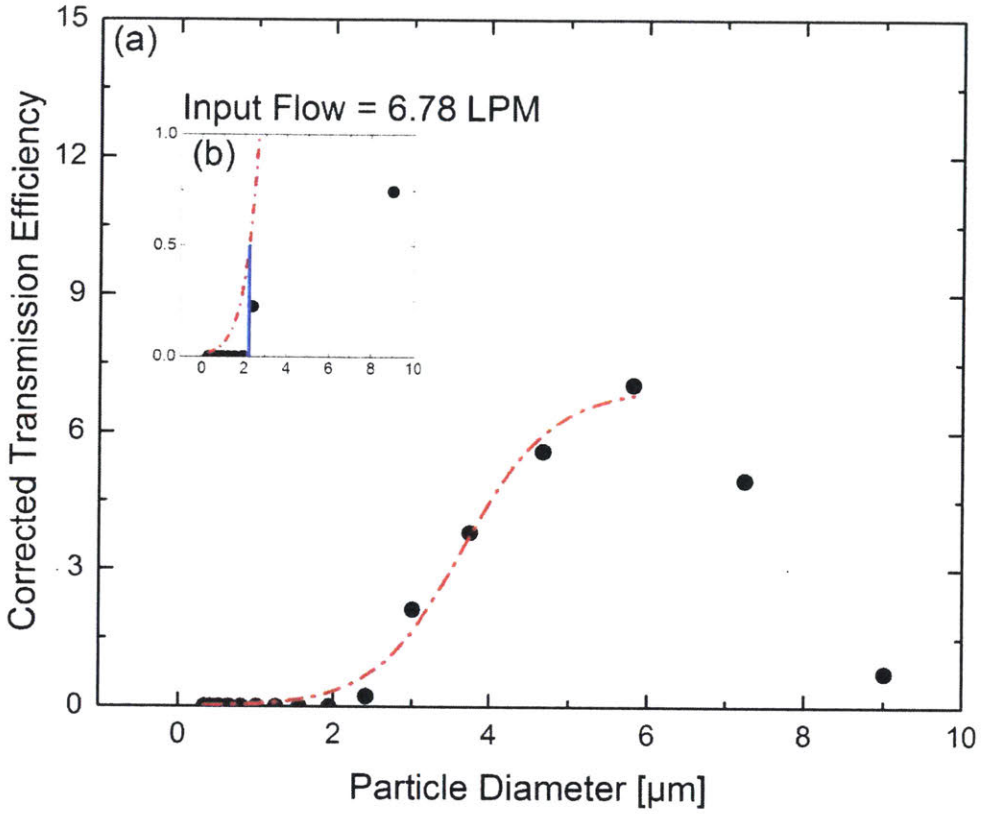

Figure C6 **A:** The transmission efficiency for the printed PCVI at an input flow of 6.78 LPM. **B:** The printed PCVI with an input flow of 6.78 LPM had a D50 value of approximately 2.2 µm.

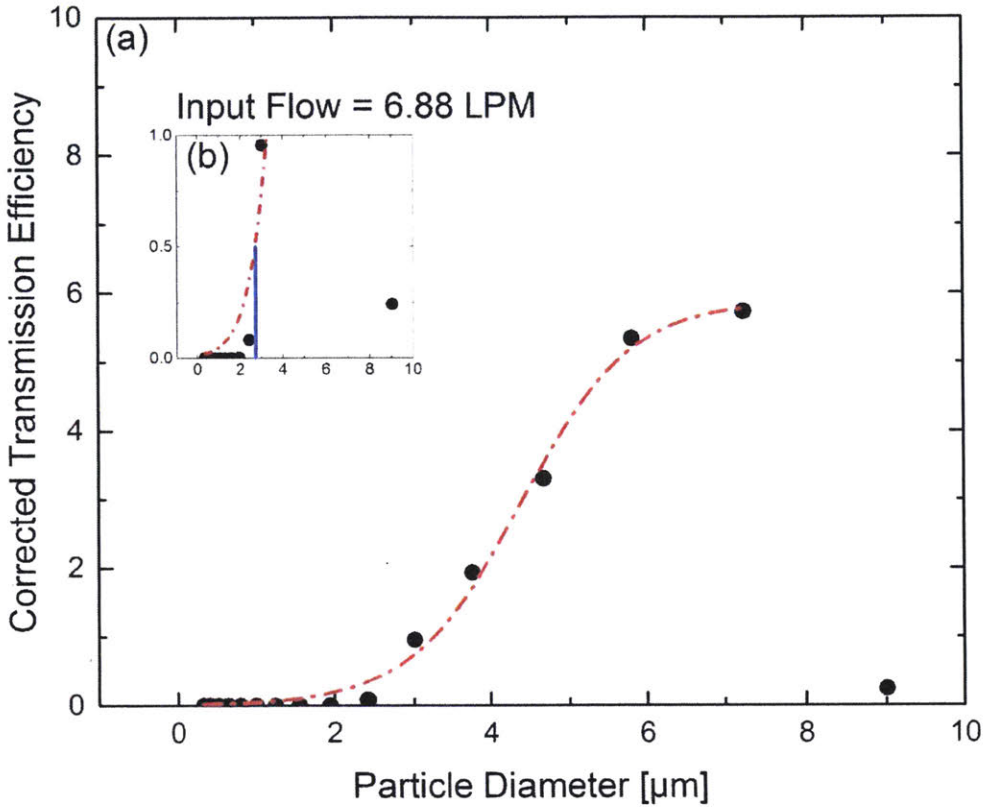

Figure C7 **A:** The transmission efficiency for the printed PCVI at an input flow of 6.88 LPM. **B:** The printed PCVI with an input flow of 6.88 LPM had a D50 value of approximately 2.7 µm.

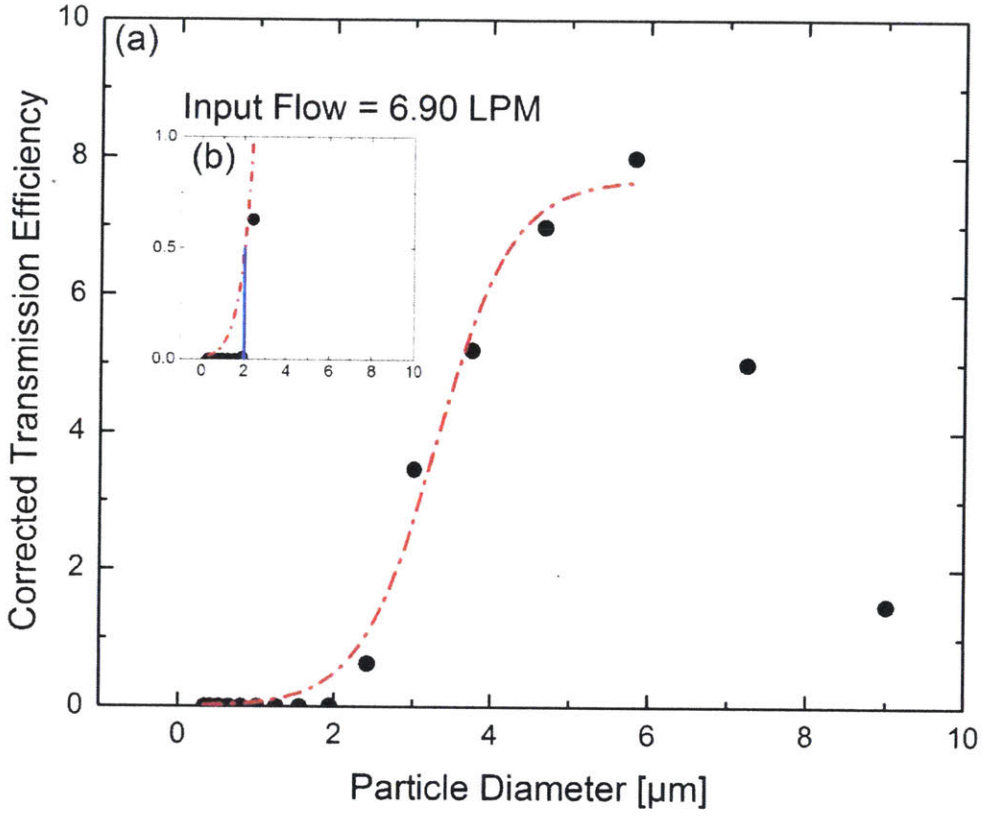

Figure C8 **A:** The transmission efficiency for the printed PCVI at an input flow of 6.90 LPM. **B:** The printed PCVI with an input flow of 6.90 LPM had a D50 value of approximately 2.0 µm.

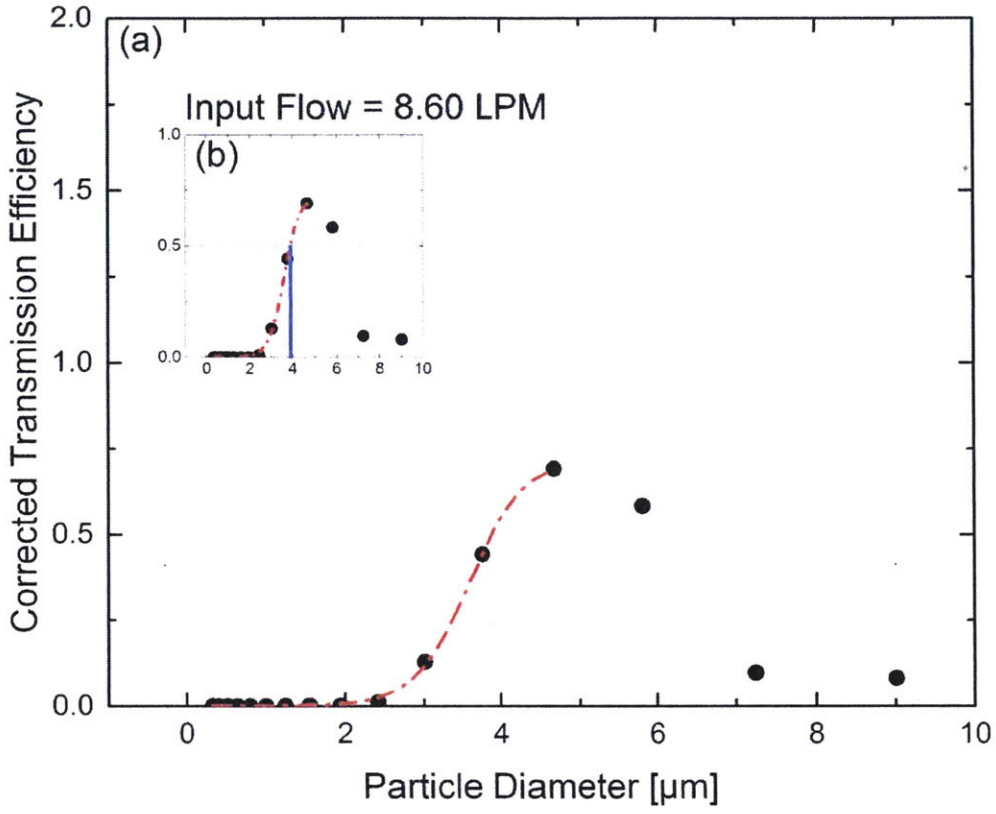

Figure C9 **A:** The transmission efficiency for the printed PCVI at an input flow of 8.60 LPM. **B:** The printed PCVI with an input flow of 8.60 LPM had a D50 value of approximately 3.9 µm.

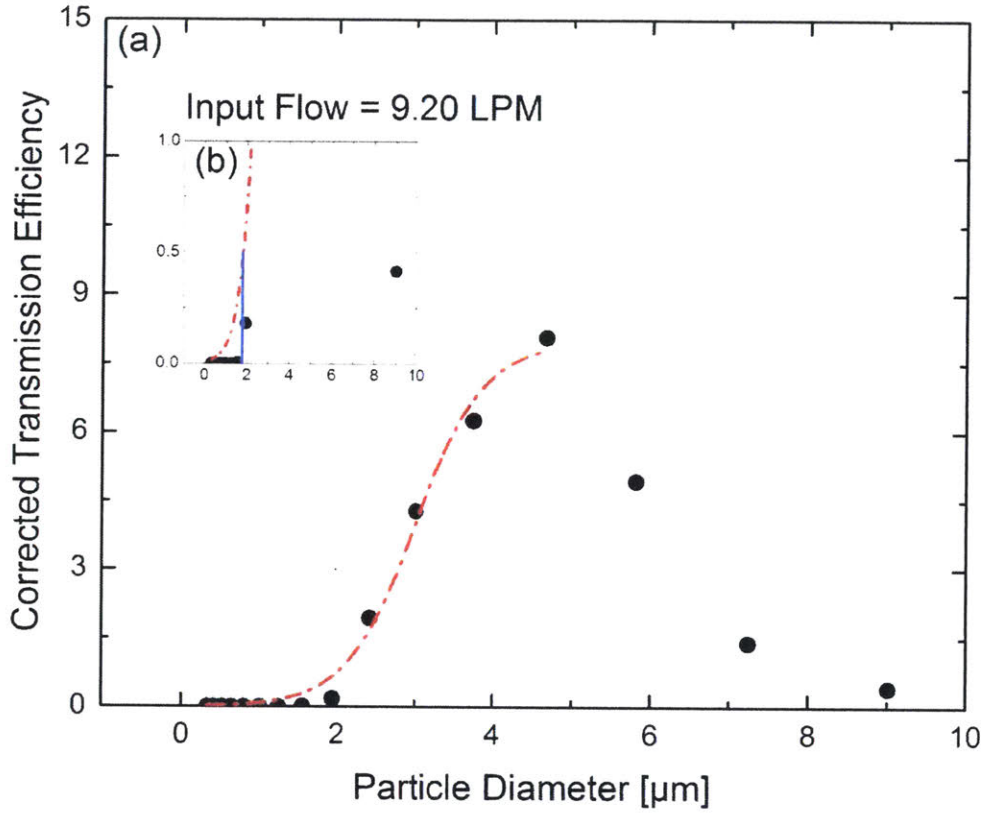

Figure C10 **A:** The transmission efficiency for the printed PCVI at an input flow of 9.20 LPM. **B:** The printed PCVI with an input flow of 9.20 LPM had a D50 value of approximately 1.8 µm.

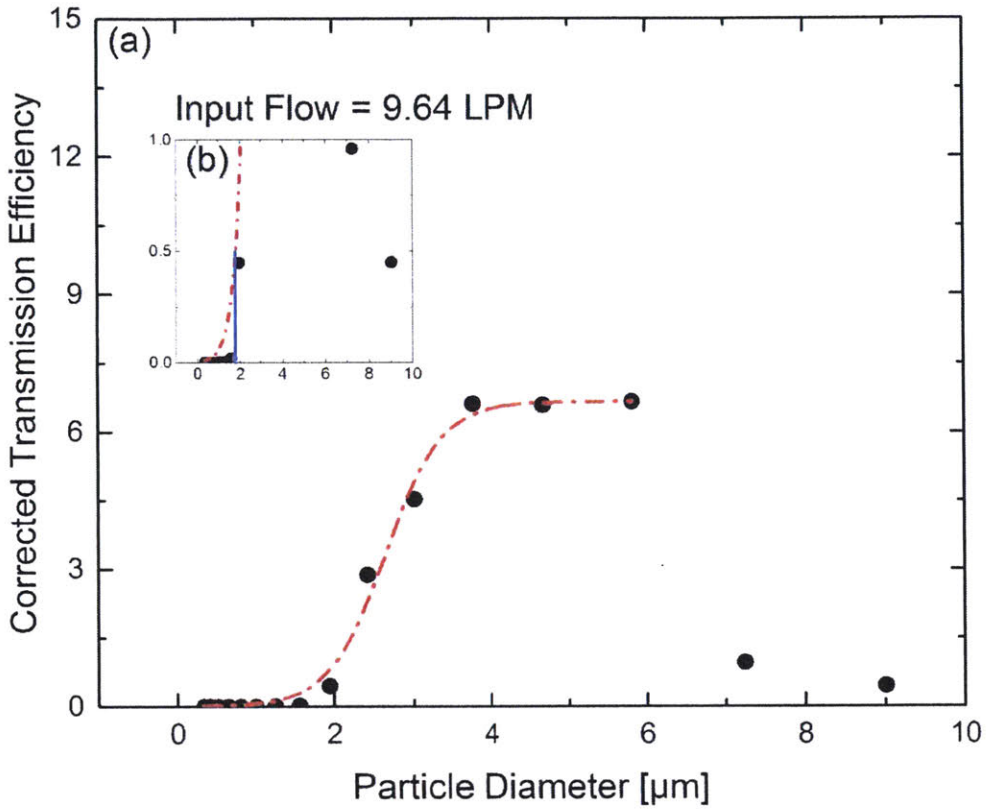

Figure C11 **A:** The transmission efficiency for the printed PCVI at an input flow of 9.64 LPM. **B:** The printed PCVI with an input flow of 9.64 LPM had a D50 value of approximately 1.7 µm.

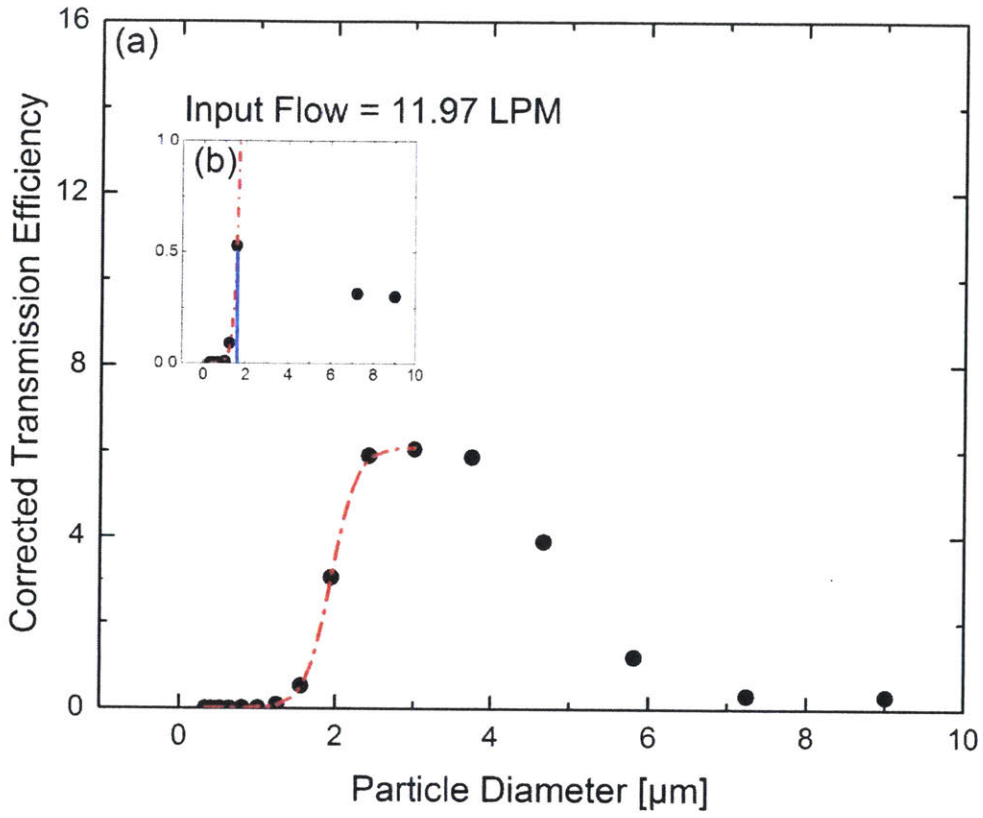

Figure C12 **A:** The transmission efficiency for the printed PCVI at an input flow of 11.97 LPM. **B:** The printed PCVI with an input flow of 11.97 LPM had a D50 value of approximately 1.54 µm.

D. SOLIDWORKS DESIGNS

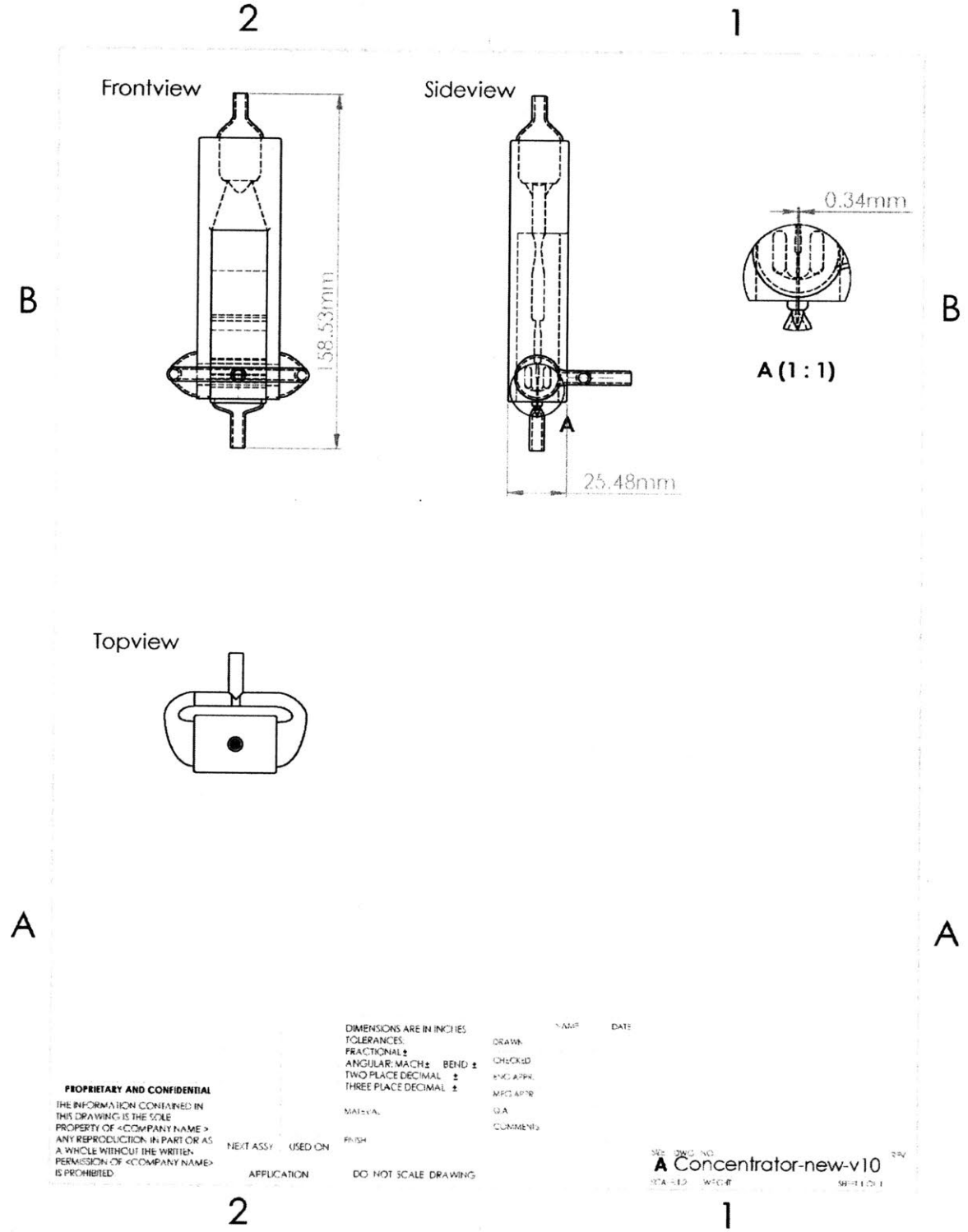

Figure D1 The cross-sections for the concentrator used to make the printed concentrator tested in this project. This 3D model of the concentrator was converted to PreForm and printed in the Form2.

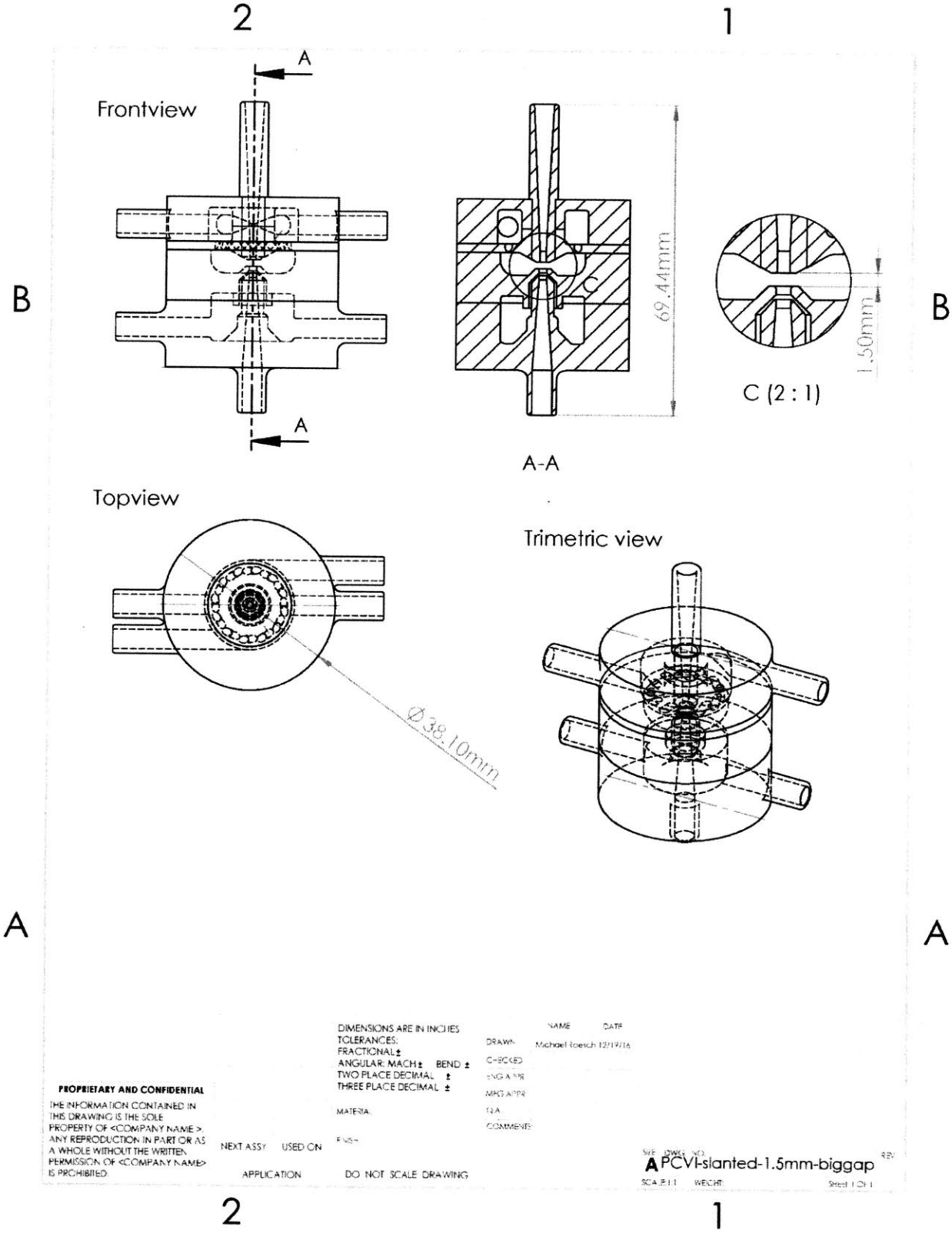

Figure D2 Multiple views of the PCVI model created in Solidworks. This design incorporates the slanted inlet nozzle. This model of the PCVI was used in all tests for this project.